9-2016

Interpreting Southern California Arc Geochemistry by Multivariate and Spatial Methods

Lance R. Pompe

LOMA LINDA UNIVERSITY
School of Medicine
in conjunction with the
Faculty of Graduate Studies

Interpreting Southern California Arc Geochemistry by Multivariate and Spatial Methods

By

Lance R. Pompe

A Thesis submitted in partial satisfaction of
the requirements for the degree
Master of Science in Geology

September 2016

Each person whose signature appears below certifies that this thesis in his/her opinion is adequate, in scope and quality, as a thesis for the degree Master of Science.

_____, Chairperson
Benjamin L. Clausen, Adjunct Associate Professor of Geology

_____
William K. Hayes, Professor of Biology

_____
Kevin E. Nick, Associate Professor of Geology

ACKNOWLEDGEMENTS

My deepest gratitude goes to my advisor, Dr. Ben Clausen. His scientific knowledge, guidance and patience made this project possible. I would like to express my appreciation to my committee members for their advice and input, Dr. Kevin Nick for help with defining the goals and aims, and Dr. Bill Hayes for the excellent multivariate statistics course and materials.

The other members of the "hard rock" team, Ana Martinez and Luciano Gonzalez have been helpful in many ways. Their friendship will always be remembered. Allan and Jamey Cooper assisted with statistical issues. Ed Santos encouraged me to use the R statistical package on more than one occasion, and I am glad I finally listened. Thank you to Dr. Leonard Brand and Dr. Paul Buchheim for ensuring that I had the financial resources to complete the program. Lastly, my sincere appreciation goes to my wife Mogi, for her encouragement and support throughout this project.

CONTENT

FIGURES

Figure Page

TABLES

ABBREVIATIONS

alr	Additive log-ratio
clr	Centered log-ratio
CODA	Compositional data analysis
CSC	Constant sum constraint
EDA	Exploratory data analysis
ETZ	Eastern transitional zone
EZ	Eastern zone
GIS	Geographic information system
HREE	Heavy rare earth element
ICP-MS	Inductively coupled plasma mass spectrometry
ilr	Isometric log-ratio
LA-ICPMS	Laser ablation inductively coupled plasma mass spectrometer
LREE	Light rare earth element
MCD	Minimum covariance determinant
MORBs	Mid-ocean ridge basalts
OIBs	Ocean island basalts
PC	Principal component
PCA	Principal component analysis
ppm	Parts per million
PRB	Peninsular Ranges batholith
REE	Rare earth element

Sr_i	Initial strontium = $^{87}Sr/^{86}Sr \mid_i$
UPZ	Upper plate zone
WTZ	Western transitional zone
WZ	Western zone
XRF	X-ray fluorescence

ABSTRACT OF THE THESIS

Interpreting Southern California Arc Geochemistry
by Multivariate and Spatial Methods

by

Lance R. Pompe

Master of Science, Graduate Program in Geology
Loma Linda University, September 2016
Dr. Benjamin L. Clausen, Chairperson

Exploratory data analysis methods of multivariate statistical techniques and spatial visualization are emerging trends in understanding big datasets. In this project, these techniques are applied to a large igneous geochemical dataset from the southern California segment of the Mesozoic Cordilleran arc to better understand magmatic and plate tectonic processes at a subduction zone. A set of 287 granitic samples collected by Baird and Miesch (1984) from the Peninsular Ranges batholith is analyzed for 38 geochemical elements. Patterns in both the geochemical variation and the spatial variation of this dataset are explored.

Since geochemical data are compositional in nature, special treatment is needed in analyzing them. Robust principal component analysis for compositional data is used to summarize the 38 geochemical variables into three principal components that are visualized using biplots. The first three principal components appear to be related to extent of differentiation, magma source depth, and possibly solubility, respectively. The first principal component (PC1) accounting for 56.7% of the explained variance, arranges the elements in order of incompatibility. The main associations of PC2 (17.3% of

explained variance) are groupings of rare earth elements, along with Y and Sr – suggesting the effect of deep garnet and shallow plagioclase fractionation in response to pressure and therefore depth. A weak association of soluble elements is found in PC3 (6.7% of explained variance).

Spatial geochemical variation is explored by mapping the standard geochemical parameters related to the principal component interpretations as well as the three principal components, and then comparing them. Extent of differentiation is mapped using SiO_2 and PC1 and resulting maps show similar patterns. Magma source depth is mapped using Sr/Y, La/Yb and PC2 and similar patterns are found. Alkalinity and possibly solubility and mobility is mapped using K_2O/SiO_2 and PC3, but these maps do not share similar patterns. Using the exploratory data analysis methods of multivariate analysis and spatial visualization is helpful in understanding geochemical patterns and trends in subduction zones.

CHAPTER ONE

INTRODUCTION AND BACKGROUND

Overview

> "I want to know how God created this world. I am not interested in this or that phenomenon, in the spectrum of this or that element. I want to know his thoughts, the rest are details."
>
> Albert Einstein

An understanding of the Earth's large continental batholiths is essential for developing models for the nature and history of plate tectonics and the continental crust (Hill, 1984). The Cordilleran arc of western North America is characterized by Mesozoic batholiths comprising extensive belts of granitic plutons that are interpreted to have been emplaced during episodes of convergence between oceanic plates to the west and the North American plate (**Figure 1**). These continental arc batholiths contributed extensively to the growth of the North American continental crust. Numerous large geochemical datasets from these batholiths have been collected over the past few decades and typically contain hundreds to thousands of samples of as many as 50 elemental and isotopic variables. These data contain a wealth of information about magmatic conditions and processes, justifying the effort and expense required to collect them.

Many studies have linked specific geochemical variables to subduction zone magmatic properties, such as differentiation extent, magma source depth and crustal contamination (Gromet and Silver, 1987; Kistler, 2003; Tulloch and Kimbrough, 2003). Traditional methods of interpreting these large datasets rely on analyzing relationships among the many geochemical variables using variation diagrams, with some of the most popular being bivariate plots and spider diagrams.

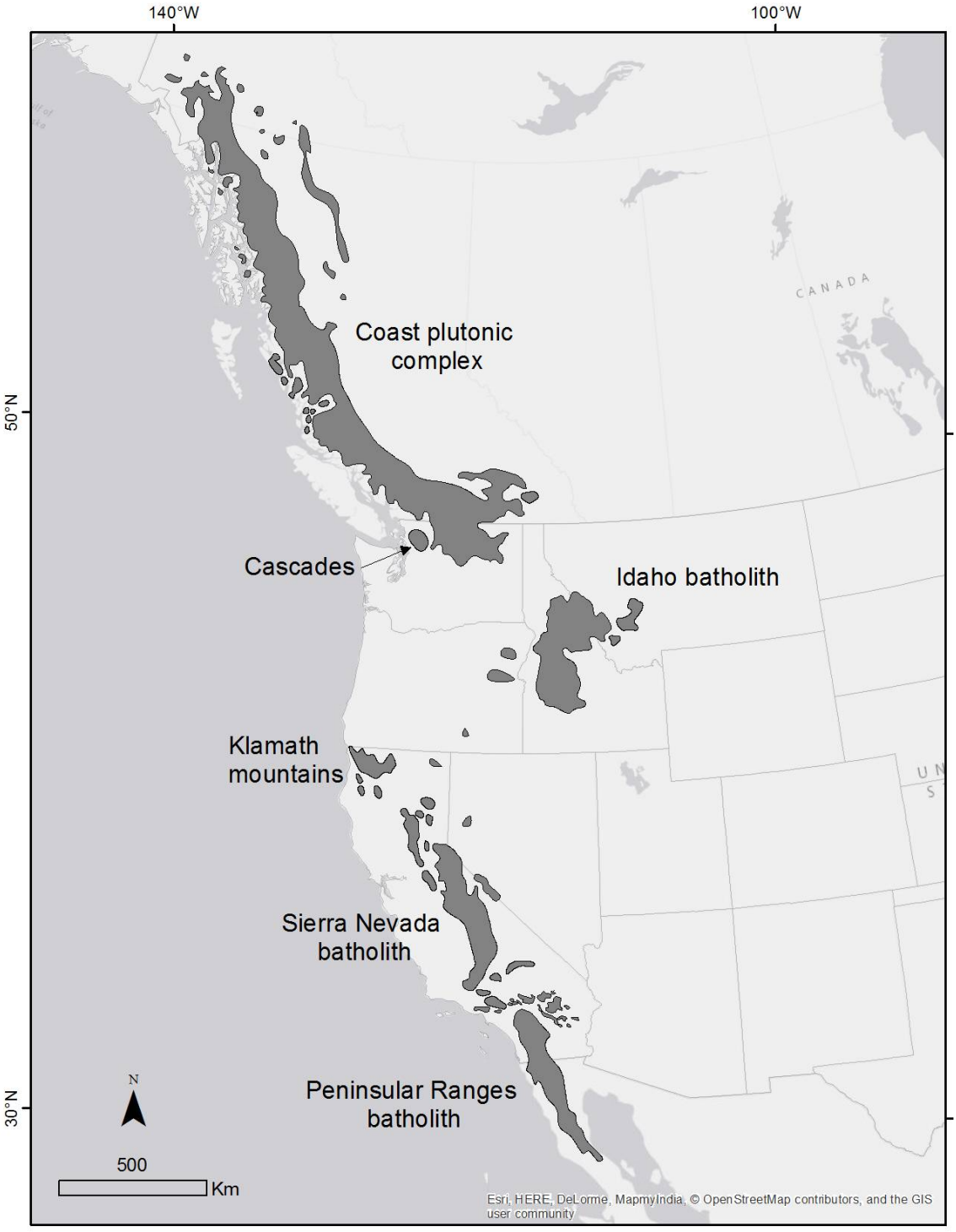

Figure 1. Cretaceous granitic batholiths along the western margin of North America. After Paterson et al. (2011) and Miller (2014).

In addition to these diagrams, geoscientists have a number of powerful data mining tools. Data mining uses various methods to evaluate data for associations, structures, and patterns. This approach has been used successfully in mineral exploration and environmental geochemistry, as well as in the fields of social, medical and biological sciences. Data mining tools include multivariate statistical analysis and machine learning techniques combined with spatial analysis to explore patterns in both the variable (element or isotope) and spatial (geographic location) domains. Exploratory multivariate data analysis techniques in combination with a spatial analysis approach like geographic information system (GIS) interpolation can greatly improve the visualization and interpretation of a geochemical dataset. Visualization is an effective way of recognizing patterns in data since the human eye is far more effective at discerning patterns from pictures than from tables of numbers (Grunsky, 2010; Pawlowsky-Glahn and Buccianti, 2011).

Multivariate analysis is the appropriate approach to investigate relationships and potential interactions among all variables in a dataset simultaneously, allowing a more comprehensive understanding than would be possible when considering variables in isolation or in pairs. Principal component analysis (PCA) is an exploratory multivariate method that is very effective at reducing a large number of variables into a small number of more easily interpretable components.

Virtually all geochemical data are compositional in nature, with the measured elemental concentrations being parts of a whole. These data sum to a constant, known as the constant-sum constraint (Kucera and Malmgren, 1998). Compositional data have a restricted sample space (since they do not vary independently) with the result that the

standard multivariate analysis techniques that operate in the Euclidean real sample space are not appropriate. Fortunately, transformations can be applied to "open up" compositional data to enable classical statistical multivariate analyses such as principal component analysis.

The northern Peninsular Ranges batholith (PRB) forms part of the southern California Cordilleran arc. This batholith has been extensively studied for decades, beginning with pluton descriptions and chemical analyses by Larsen (1948) and culminating in a 2014 GSA memoir, "Peninsular Ranges Batholith, Baja California and Southern California" edited by D. M. Morton and F. K. Miller. Many analyses in this volume are based on one of the most systematically sampled batholithic geochemical datasets in existence, assembled by A.K. Baird and his student E.E. Welday (Baird et al., 1979; Baird and Miesch, 1984). Baird and Welday also sampled the Transverse Ranges to the north of the Peninsular Ranges batholith, providing an additional dataset that can be used to explore the across-arc variation in igneous geochemistry after removing San Andreas Fault displacement.

The purpose of this project is summarized by considering several goals and aims:

- Goal 1: To demonstrate the usefulness of multivariate analysis for igneous petrology by identifying patterns of geochemical variation using a comprehensive dataset from the northern Peninsular Ranges batholith.
- Goal 2: To better understand the geochemical variation across a subduction zone arc in terms of varying magma production processes.
- Aim: Compare multivariate analysis results with the standard bivariate approach in order to explain magmatism in the northern Peninsular Ranges batholith by:

- Finding statistical groupings of variables and linking each of them to an appropriate geochemical interpretation.
- Graphically comparing principal components with standard geochemical parameters.

In addition to these objectives, it is hoped that insights gained from applying these techniques to geochemical data from a relatively well-studied area like the southern California arc can be useful in understanding other less well-understood batholiths.

Geologic Setting

Most Cordilleran batholiths of western North America are composite elongate belts aligned parallel to the past Cordilleran margin. The emplacement patterns are typically complex and likely resulted from changes in plate orientation and motion over time. In contrast to these complex emplacement patterns, the Cretaceous Peninsular Ranges batholith displays a relatively simple, monotonically varying pattern having little overlap with older plutonic arcs (Gromet and Silver, 1987). It is considered a classic example of subduction-related magmatism (Hill, 1984; Morton et al., 2014). The Peninsular Ranges batholith extends as a narrow (120 km wide) belt for approximately 1000 km from southern California into Baja California in Mexico. The northern boundary of the Peninsular Ranges batholith is defined by the east-west striking Malibu Coast-Cucamonga fault, the San Andreas fault, and the Banning fault (Baird and Miesch, 1984) (**Figure 2**). Emplacement proceeded from west to east (younging eastward) over a period of 51 m.y. from 126 Ma to 75 Ma (Morton et al., 2014).

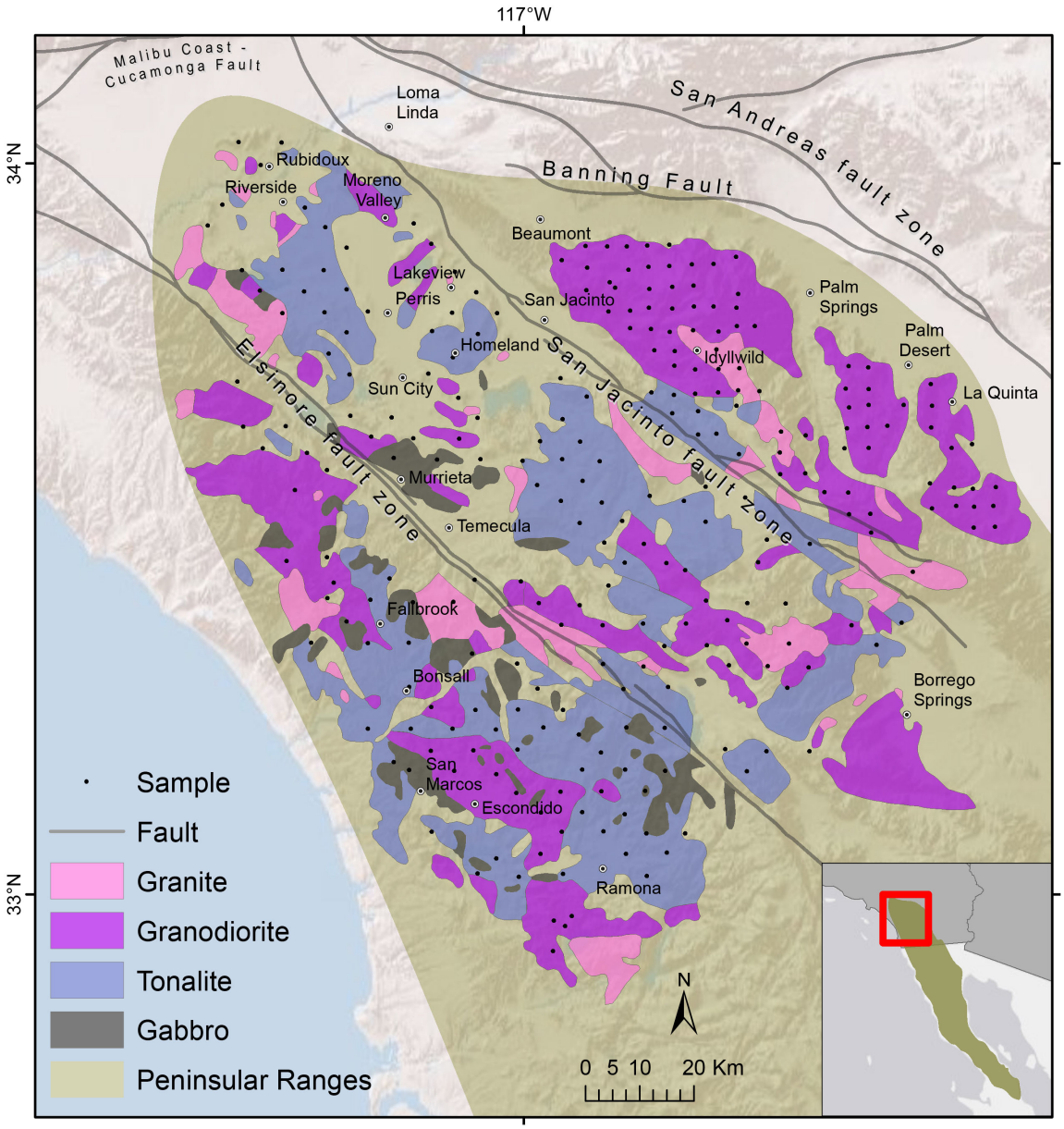

Figure 2. Pluton map of the northern Peninsular Ranges batholith showing sample locations and rock type. Sample and pluton data from Baird and Miesch (1984). Granite and tonalite categories approximately correspond to Baird's quartz monzonite and quartz diorite respectively, which were based on the igneous rock classification of Bateman et al. (1963).

The northern Peninsular Ranges batholith consists of Cretaceous and some Jurassic plutonic rocks emplaced into meta-sedimentary and meta-volcanic rocks. It is

made up of more than 100 predominantly tonalite plutons, but compositions range from gabbro to granite (Larsen, 1948; Silver and Chappell, 1988).

The right lateral San Andreas fault zone strikes northwestward from the northern margin of the Peninsular Ranges, separating the northern Peninsular Ranges batholith from the Transverse Ranges. The magnitude of movement of the strike-slip component along the associated Elsinore and San Jacinto fault zones has been determined to be relatively small (Baird and Miesch, 1984). Miller et al. (2014) demonstrated that age contours show the best alignment after restoration of an offset of 12 km for the right lateral Elsinore fault zone and 29 km for the right lateral San Jacinto fault zone. This San Jacinto offset is in agreement with 29 km of total offset calculated from contact offsets of distinctive rock types across the San Jacinto fault system by Sharp (1967).

Geologic Background

Subduction zones are an important source of information about plate tectonic and continental crust forming processes. The analysis of large geochemical and geochronological datasets provides important clues about magma chamber conditions and plate tectonic processes, such as amount of magma melting, partial melting/fractional crystallization cycles, pressure, temperature, and magma water content. Today, southern California is no longer an active subduction zone as in the Cretaceous when the oceanic Farallon plate was subducting beneath the continental North American plate. However, through geochemical data analysis, we can reconstruct, to a degree, the subduction environment and processes as they were in the Cretaceous.

This section firstly introduces basic characteristics of larger scale arc systems, including geomorphic features and temporal variation. Next, differentiation processes are discussed, followed by four important features of subduction zones that have been characterized using geochemistry, namely extent of differentiation, magma source depth, crustal contamination and alkalinity. Then, exploratory data analysis is introduced, including principal component analysis, cluster analysis, the analysis of compositional data, and spatial visualization. Finally, PRB subdivisions, W-E variation and some previous work done in the PRB using multivariate and spatial analysis is briefly described.

Arc Processes

Arc Systems and Subduction

Arc systems can be subdivided into island arcs and continental-margin arcs and are found above active or previously active subduction zones. Island arcs are formed on oceanic crust where an oceanic plate subducts beneath another oceanic plate, forming arcuate island chains, such as the Mariana and Lesser Antilles arcs. Continental margin arcs form above subduction zones where oceanic plates plunge beneath continental plates, for example the Andean and North America Cordillera and Japan arcs (Condie, 2013).

At subduction zones, the higher density subducting oceanic slab carries ocean water down with it into the mantle. As the subducting slab moves through increasing temperature and pressure zones, it dehydrates and the water enters the mantle wedge and lower crust. This water has the effect of lowering the melting temperature of the surrounding rocks, creating batches of magma through partial melting. The magma

ascends through the mantle and continental crust to form intrusive magma bodies creating plutons and batholiths, or erupts at the surface as volcanoes. Successive cycles of partial melting, crustal assimilation, and fractional crystallization tend to increasingly differentiate a lithosphere assumed to be originally homogeneous, creating the felsic granitic rocks common on continents, from the mafic mantle rocks. As a result of these processes, subduction zone geochemistry is more complex than in any other igneous environment (Condie, 2013; Winter, 2010).

Temporal Variation in Arc Magmatism

Using large geochronological datasets (categorized by U-Pb bedrock and detrital zircons) from eight segments of the American Cordillera, Paterson and Ducea (2015) showed that magmatism in arcs is clearly episodic. Periods with a high magma addition rate are called "flare-ups" and periods of little magmatic activity are termed "lulls." They noted that flare-ups and lulls exhibit "apparent wavelike patterns of waxing and waning magmatism." An active area of research is concerned with linking external factors such as changes in mantle flow, plate reconfigurations and collisions to magmatic flare-ups.

Differentiation

Chemical Fractionation

Trace elements are defined as elements that occur in quantities of < 0.1 wt. %. The interest in trace elements in igneous processes is focused on the elements located in the lower left part of the periodic table (K, Rb, Cs, Sr, Ba, the rare earth elements, Y, Zr, Nb, Hf and Ta). One of the reasons for this interest is because these elements are lithophile, and therefore are found in relatively high abundance in the Earth's crust and mantle.

Another reason is that their chemical behavior is relatively simple, being mainly a function of ionic size and charge. Other trace elements that are of interest are the first transition series elements. Although their chemical behaviors are a lot more complex, charge and size are still important. Many of these elements are preferentially incorporated into the solid in Mg-Fe silicate minerals and are called "compatible elements" (Goldschmidt, 1937; White, 2013; Winter, 2010). **Figure 3** plots the elements analyzed for the PRB by ionic size and charge.

Chemical fractionation is the uneven distribution of an ion between two competing equilibrium phases. The partitioning of elements between the melt and solid phases results in incompatible elements being concentrated in the melt and compatible elements being concentrated in the solid. The manner in which elements are partitioned between the solid and melt can be better understood by considering Goldschmidt's rules of element distribution (Goldschmidt, 1937; Ringwood, 1955):

1. Two ions with the same valence and similar radius (radii differing by less than approximately 15%) should exchange easily and enter a solid solution in amounts equal to their overall proportions.
2. If two ions have a similar radius and the same valence, the smaller ion is preferentially incorporated into the solid over the liquid.
3. If two ions have a similar radius but different valence, the ion with the higher charge is preferentially incorporated into the solid over the liquid.

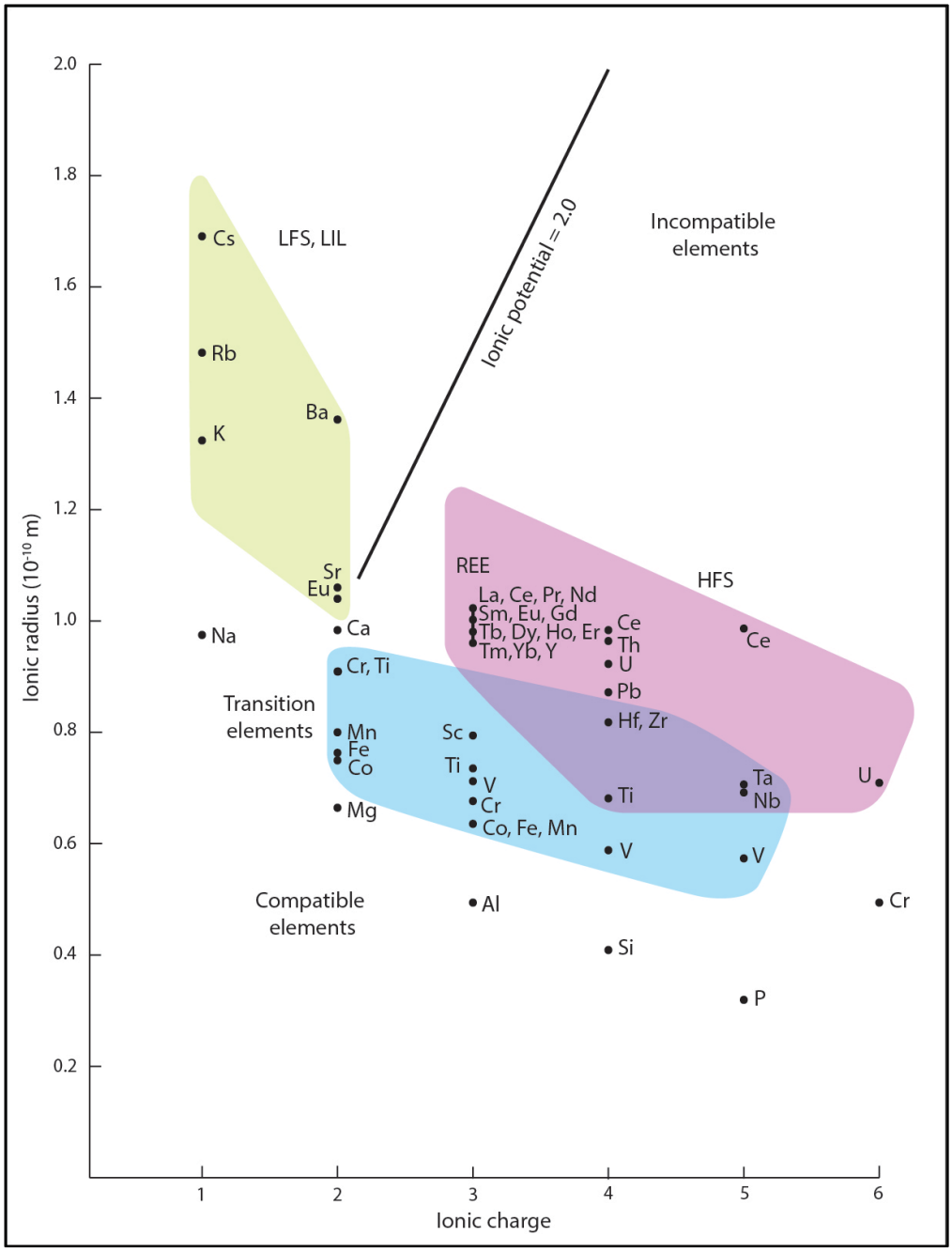

Figure 3. Ionic radius plotted against ionic charge for the geochemical variables of interest in the northern Peninsular Ranges batholith data. Compatible elements are towards the low ionic charge, small ionic radius corner. The incompatible elements are subdivided into low field strength (LFS) and high field strength (HFS) elements by a charge/size ratio of 2.0. Although Si and Al plot in the compatible area, they are unique and display their own relationships. Adapted from Rollinson (1993) with ionic radii from Railsback (2012).

Incompatible elements can be divided into two subgroups (Rollinson, 1993), see **Figure 3**:

1. Smaller, highly charged high field strength (HFS) elements (rare earth elements (REE), Th, U, Ce, Pb^{4+}, Zr, Hf, Ti, Nb, Ta).
2. Low field strength large ion lithophile (LIL) elements (K, Rb, Cs, Ba, Sr, Eu), which are more mobile, particularly if a fluid phase is involved.

Partial Melting

Rocks in the upper mantle region known as the asthenosphere or seismic low velocity zone are close to the point of partial melting and behave in a ductile fashion. The ductile nature of the asthenosphere facilitates the movement of tectonic plates above and the asthenosphere is in turn impacted by tectonic plates through subduction. Asthenosphere rocks begin to melt in specific circumstances – in response to increased temperature, decreased pressure or compositional change, such as the introduction of volatiles, especially water. Water introduced into the mantle wedge in subduction zones by the dehydration of descending slabs triggers partial melting. Since rocks are composed of different rock-forming minerals, minerals with lower melting temperatures begin to melt first.

Partial melting occurs when a rock has different solidus (temperature at which melting begins) and liquidus (temperature above which a rock is completely liquid) temperatures. The resulting magma is squeezed out of the parent rock and begins to move toward the surface since it has a lower density than the surrounding rocks. The

composition of this melt is not the same as the bulk composition of the parent rock, due to the effect of chemical fractionation.

During partial melting, the degree of fractionation between compatible elements in the solid and incompatible elements in the melt is a function of the amount of melting. If the amount of partial melting is slight (only a few percent, for example) a higher degree of fractionation will occur than if the amount of partial melting is greater (Grove et al., 2012; Winter, 2010).

Fractional Crystallization

As ascending melts cool and interact with country rock, minerals with the highest melting points or lowest solubilities, such as olivine and pyroxene, crystalize out of the melt first. The last minerals to crystalize are those with the lowest melting points or highest solubilities, with silica content in the melt increasing over time. Bowen (1922) experimented on the order in which minerals crystalized from a melt to determine this reaction series. During the process of fractional crystallization, the melt becomes increasingly enriched in incompatible elements by the same mechanism operating in partial melting – chemical fractionation.

Subduction Zone Geochemistry

Extent of Differentiation: SiO_2

Felsic rocks of the continental crust with higher SiO_2 concentrations are evolved or differentiated from the more mafic mantle which has a lower SiO_2 concentration. As these rocks have undergone one or more cycles of partial melting and fractional crystallization, they are enriched in the incompatible elements. Although the volume of

the continental crust is equivalent to only about 0.6% of the volume of the mantle, it contains 30 – 50% of the earth's highly incompatible trace elements. A complementary pattern of depletion in these elements is found in the upper mantle, which suggests extraction of these elements through partial melting-fractional crystallization cycles (Hofmann, 1988). The extent of differentiation is typified by the SiO_2 concentration.

Crustal Contamination: Sr_i

A mafic mantle-derived magma that moves through more felsic continental crust will become enriched in incompatible elements as it melts surrounding crustal rock and mixes with it (crustal enrichment or contamination). This enrichment also occurs when rocks undergo cycles of partial melting and fractional crystallization. Isotopic methods can be used to distinguish between crustal and mantle derived enrichment signatures since isotopes are not affected by the fractionating processes of partial melting and fractional crystallization that elements experience during magma ascent and emplacement (Faure and Powell, 2012). However, mantle plumes may produce isotopic signatures similar to the crust and it is suggested that crustal or mantle contributions to magmatism can be recognized by observing the products of processes such as magma mixing or crustal assimilation (Hawkesworth et al., 1984; Thirlwall and Jones, 1983).

It is generally accepted that initial strontium ($^{87}Sr/^{86}Sr \mid_i$ or Sr_i) values are an indicator of the continental crustal component in magma (Faure and Powell, 2012). Initial strontium values greater than 0.706 are thought to indicate a predominantly continental crust magma source while values below 0.706 suggest a largely mantle source. For example, Langenheim et al. (2004) looked at the preexisting structure within the

Peninsular Ranges batholith by analyzing geophysical (gravity and magnetic field) anomalies and Sr_i data. A correspondence was found between the geophysical and Sr_i data, suggesting different prebatholithic geologic blocks underlying the batholith, with the west being denser, more mafic, and yielding Sr_i values generally lower than 0.706, and the east being less dense, more felsic, and yielding Sr_i values generally higher than 0.706.

Magma Source Depth: REE and Sr/Y

Researchers have recognized that arc magmatic geochemistry is sensitive to Moho depth (Chapman et al., 2015). Globally, the Moho defines the crust-mantle boundary; however in subduction zones the Moho is associated with both the subducting slab and the overriding plate and approximately coincides with Wadati-Benioff seismicity (a planar zone of seismicity corresponding to the down-going slab in subduction zones) (Bostock, 2013).

Some major oxides of mafic arc rocks, such as Na_2O and CaO, correlate with crustal thickness at global scales; however these correlations break down where crustal thickness exceeds 45 km. MnO is likely the only major element that correlates well with crustal thickness, but it has a small variation in the calc-alkaline rocks typical of continental arcs, resulting in a weak correlation (Leeman, 1983; Profeta et al., 2015).

Various light rare earth element (LREE) and heavy rare earth element (HREE) ratios have been used to quantitatively infer the depth of magma fractionating processes. By plotting REE spider diagrams, the differences in partition coefficients between light and heavy REEs can be compared. For crystallization below the garnet stability pressure

of 10 - 12 kbar (or depth > 33 – 40 km), there is a variation of three orders of magnitude in the partition coefficient of garnet between the lightest and heaviest REEs (see **Figure 4**) (Carrol and Wyllie, 1990; Morton et al., 2014; Rollinson, 1993).

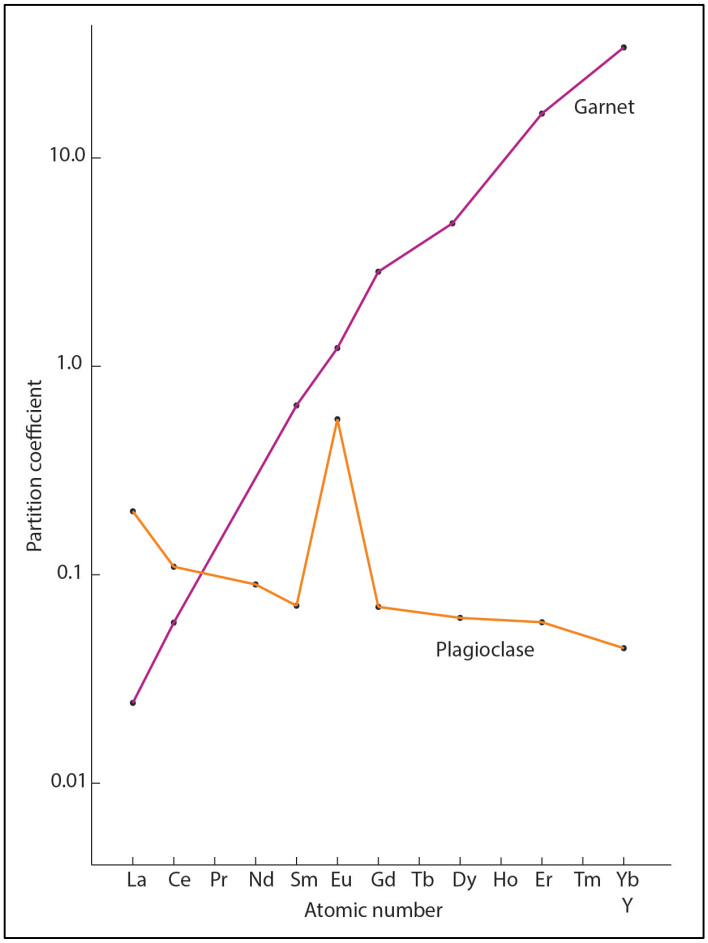

Figure 4: Partition coefficient plotted against atomic number for REE in garnet and plagioclase in basaltic melts. After Rollinson (1993).

Depth can be estimated from all the rare earth elements (La/Yb) or separately for the LREE ratio La/Sm and HREE ratio Gd/Yb. As magma source depth increases, La/Sm and Gd/Yb increase with fractionation (Morton et al., 2014).

The Sr/Y ratio has also been used to distinguish between fractionation processes occurring at depth and those at shallow levels due to differences in the partition coefficient between those elements for the residual (solid) and melt phases (Lee et al., 2007). At depth, in the high pressure garnet stability zone, Y and the HREEs are separated out of the melt during partial melting and fractional crystallization into garnet (Y has behavior similar to Yb, but is more convenient to measure due to higher concentrations). Thus, the melt is strongly depleted in yttrium and the HREEs. At shallow depth, yttrium and the HREEs are not depleted in the melt, since garnet is not stable here. In the shallow plagioclase stability zone (< ~3 kbar pressure or depth of < ~10 km), strontium strongly partitions into plagioclase, substituting for calcium. Note the relatively flat partition coefficient curve for plagioclase in **Figure 4** (except for Eu which substitutes for Ca). At greater depths, plagioclase is unstable and strontium preferentially enters the liquid phase (Morton et al., 2014; Profeta et al., 2015).

Chapman et al. (2015) suggest that Sr/Y is a viable parameter for reconstructing crustal thickness through time in calc-alkaline convergent orogenic systems. Profeta et al. (2015) correlated whole rock concentrations of Sr/Y and La/Yb from global and regional samples taken from modern Pacific subduction zone magmatic arcs with the purpose of estimating crustal thickness. Using a large global geochemical database of geologically young arc rocks, knowledge of global crustal thickness, and a regional dataset from the southern Andean zone where crustal thickness varies greatly over a short distance, they found Sr/Y and La/Yb values correlated well with Moho depth (R^2 = 0.9 and 0.72 respectively). The relationship between Sr/Y (y) and the Moho depth (x) in kilometers was defined by the equation $y = (0.9 \pm 0.06)x - (7.25 \pm 1.89)$.

Alkalinity: K_2O

A mafic magma from a mantle source high in iron and magnesium evolves through a series of compositions in an alkaline or subalkaline magma series to produce a basalt or gabbro which further differentiates to become a felsic magma. Two subdivisions of the subalkaline magma series are the tholeiitic and calc-alkaline series (Le Maitre et al., 2005; Tilley, 1950). Tholeiitic magmas are produced from 20-40% partial melting at a depth of 30-40 km while calc-alkaline magmas result from ≤ 20% partial melting at a depth of ≥ 40 km. Although both series produce gabbro, tonalite, granodiorite, and granite (as well as their extrusive counterparts: basalt, andesite, dacite and rhyolite), there are distinct mineralogical and chemical differences between them. Tholeiitic magmas are associated with divergent boundaries, such as mid ocean ridge basalts (MORBs), while calc-alkaline magmas are restricted to subduction-related plate tectonic processes. Magma series are an important part of understanding petrogenesis and the historic tectonic framework of an area (Winter, 2010).

Spatial and temporal trends in magma series of island arcs have been noted by Kuno (1959). Although several processes are known to increase K_2O concentrations, the concentration of K_2O in volcanic lava was found to be related to the depth from the volcano to the Wadati-Benioff zone. This has been called the K-h relationship (Kuno, 1959). Low potassium tholeiites occur close to the trench while higher potassium calc-alkaline magmas are found further from the trench, corresponding to a deeper source. The same trend has been found for continental arcs (Tatsumi and Eggins, 1995; Winter, 2010).

Exploratory Data Analysis (EDA) Background

Exploratory data analysis (EDA) applied to granitic geochemistry datasets involves analyzing multivariate geochemical data to detect trends that can give insights into geochemical processes. EDA methods include, amongst others, principal component analysis, cluster analysis, and spatial interpolation. Grunsky (2010) provides a detailed review of these and other EDA techniques.

Principal Component Analysis

Geochemical data are typically composed of a large number of geochemical variables measured over a large number of samples. These data are arranged in tabular form called a data matrix, with each sample representing a row of the data matrix and each variable a column. Factor analysis is a class of analysis methods, which includes principal component analysis, that aims to achieve a parsimonious description of the data matrix, in other words to simplify it (Klovan, 1975).

Principal component analysis is a very popular exploratory multivariate statistical technique that aims to reduce the number of variables necessary to describe the observed variation into a small number of principal components (Abdi and Williams, 2010; Jolliffe, 2014). Frequently used in the social sciences, the technique is also often used in engineering, computer vision, and many other applied science applications that involve large volumes of high-dimensional data (Chavez Jr and Kwarteng, 1989; De la Torre and Black, 2001). PCA algorithms implement mathematical dimensionality-reduction using singular value decomposition of a data matrix (Van den Boogaart and Tolosana-Delgado, 2013). The underlying mathematical objective is to represent as much of the total variation as possible by forming uncorrelated (orthogonal) linear combinations of the

original variables—the principal components. Principal components are ordered in terms of decreasing amount of variance represented. The first principal component, PC1 represents the maximum amount of variance and is defined by:

$$\text{PC1} = a_{11}x_1 + a_{12}x_2 + a_{13}x_3 + \ldots + a_{1p}x_p$$

where x_i is the i^{th} original variable, a_{1i} is the weight assigned to the variable for the first principal component and p is the total number of original variables.

The amount of total variance explained by a principal component is termed the eigenvalue, with the total amount of variability equal to the number of original variables and each original variable contributing one unit of variability to the total. PCA output includes a matrix of factor loadings and a list of communalities. A factor loading is the Pearson correlation coefficient between an original variable and a principal component (a_{ij} in the equation above). The sum of squared factor loadings indicates the percentage of the variance in an original variable that is explained by a factor. Examining factor loadings is the key to understanding the underlying nature of a particular principal component. Variables typically have a large loading on only one factor, and much smaller loadings on all the other factors. Each variable has an associated communality representing the proportion of variability explained by the principal components for that variable. Principal component scores can be computed from the factor loadings to enable the original data to be expressed in terms of the calculated principal components. PC scores are the scores of each case (row) on each principal component (column). The PC score for a given case for a given principal component is computed by taking the case's standardized score on each variable, multiplying by the corresponding factor loading of the variable for the given factor, and summing these products.

Other important PCA outputs are eigenvalues and eigenvectors. An eigenvalue is the column sum of squared loadings for a principal component, conceptually representing the amount of variance accounted for by a principal component. A principal component is described by an eigenvector made up of the coefficients of the variables related to it (Davis and Sampson, 1986; Joreskog et al., 1976; Mertler and Vannatta, 2002).

Although for PCA it is not necessary to test the assumptions of multivariate normality and linearity as with some other multivariate techniques, the technique does work best on normal distributions with linear relationships amongst the variables. It is often helpful to apply a transformation to a non-normal or non-linear distribution (Mertler and Vannatta, 2002). Since PCA is based on the mean and sample covariance matrix of the data, it is very sensitive to outliers. The usual approach is to identify and remove multivariate outliers using a technique like Mahalanobis distance. An alternative approach is to use robust PCA to reduce the sensitivity of PCA to outliers. A construct known as the MCD (minimum covariance determinant) estimator has a high resistance to outliers and is commonly used to implement robust PCA (Filzmoser et al., 2009; Hubert and Engelen, 2004).

The first decision to make when interpreting PCA results is determining the number of principal components to retain. Several methods can be used to do this. One of the most widely used criteria, known as *Kaiser's rule*, recommends retaining principal components that have an eigenvalue greater than one. Another method for determining the number of principal components to retain is known as the *scree test*. A scree plot depicts the magnitude of each eigenvalue plotted against its ordinal number. The appropriate number of principal components to retain is determined by looking for the

knee in the curve, the point at which it appears to level off. This is usually after the first two to four principal components. Principal components after the knee have relatively small and similar-sized eigenvalues, and should be ignored (Mertler and Vannatta, 2002).

Ideally, each principal component would be interpreted as describing a geological process or be related to a geological condition. Usually the first two or three principal components that account for most of the variation have good correlation with the interpreted process, and then successive principal components show increasing mixtures of several processes and are more difficult to interpret (Grunsky, 2010).

Cluster Analysis

Cluster analysis methods can be used to detect groups of multivariate data that cannot easily be observed in simple scatter plots or through methods like PCA. Clustering algorithms such as K-means clustering aim to find natural groupings within multivariate data (Alférez et al., 2015; Ding and He, 2004). The correlation coefficient (R-mode) is usually used as the measure of similarity for performing cluster analysis. K-means cluster analysis begins with a 'guess' at the cluster centers, and then each sample is assigned to the cluster center that it is closest to. New cluster centers are created based on the previous ones and the process iterates until stable centers are found. Less than optimal clustering can occur if the guess at the initial number of centers is too low or too high.

Cluster analysis methods like K-means clustering can be applied to principal component scores created from PCA. The application of cluster analysis can give additional insight into how the interpreted principal component processes are related (Grunsky, 2010).

Compositional Data

Almost all geochemistry data are compositional in nature, meaning they sum to a constant, such as 1% or 100%, a mathematical property known as the constant-sum constraint (CSC) (Kucera and Malmgren, 1998). Due to the CSC, compositional data have a strongly negative-biased correlation structure, resulting in many multivariate techniques, such as PCA, being unreliable. This problem was first recognized by Pearson (1897), who noticed the presence of spurious correlations that affect all data that measure some part of the same whole, such as parts per million (ppm), percentages or proportions. In addition to being confined to the non-negative numbers ($\mathbb{R}_+^D$, variables that only range in the positive part of real space), compositional data are further restricted by being scaled by the total of the parts of the composition.

Due to these restrictions, Chayes (1971) described these data as being 'closed.' Variables in closed datasets are not able to vary independently of each other, and this is particularly noticeable in a variance-covariance structure such as is used in PCA (Aitchison, 1986). Compositional data can be mathematically represented for D parts as restricted to a sample space called the simplex, S^D (also known as the Aitchison geometry):

$$S^D = \left\{ x = (x_1 x_2 \dots x_D) : x_i > 0 \ (i = 1,2 \dots D), \sum_{i=1}^{D} x_i = K \right\}$$

where K is a defined positive constant that depends on how the parts are measured.

Standard statistical analyses assume that the sample space is $\mathbb{R}^D$ with D dimensions that have values that can range to $\pm\infty$, which is not the case with compositional data (Buccianti, 2013; Pawlowsky-Glahn et al., 2007). With compositional data, only statements about ratios of parts are meaningful. However, if the same

denominator is used in ratios, such as a/x and b/x, the compositional problem remains. This has been indirectly recognized in geochemistry through the use of ratio diagrams such as ternary diagrams, showing one part decreasing as another increases (Butler et al., 2005).

The problem of the statistical analysis of compositional data remained unsolved until Aitchison (1986) introduced the log-ratio approach. Since then, compositional data analysis (CODA) has been a hot topic in statistical circles, with many researchers adopting this new approach to solve analysis problems that were recognized to have been previously tackled in the wrong manner (Butler et al., 2005; Carranza, 2011; Egozcue et al., 2003; Engle and Blondes, 2014; Filzmoser and Hron, 2008; Filzmoser et al., 2009; Flood et al., 2015; Grunsky et al., 2014; Neocleous et al., 2011; Reimann et al., 2012).

The log-ratio transformations that Aitchison (1986) proposed move compositional data from the simplex (Aitchison geometry) into the Euclidean real space (Euclidean geometry) by capturing difference in the data. For example, the difference between 5% and 15% and between 20% and 30% is 10 in both cases in the real space. The log-ratio transformation can be said to 'open up' the compositional data to allow classical statistical methods to be used in the same way they are used for standard data. The inverse transformation can then be used to interpret the results in the simplex (Aitchison, 1986; Buccianti, 2013). Aitchison (1986) originally introduced the additive log-ratio (alr) and centered log-ratio (clr) transformations as solutions. Although these transformations from the simplex into multidimensional real space solved the compositional problem, they have some shortcomings that make interpretation difficult.

The alr transformation is defined as the log of the ratio of parts over a chosen part. A composition with D parts is transformed into D-1 real components and changing the part used for the denominator will create a different alr transformation. This is known as asymmetry. In addition, the alr transformation is not an isometric transformation from the simplex, due to the loss of the part used as the denominator, making interpretation of results difficult.

The clr transformation transforms D compositional parts into D real components that add up to 0 ($\sum_{i=1}^{D} y_i = 0$ where $y \in \mathbb{R}^D$), by dividing each sample by the geometric mean of its parts and taking the logarithm. It is symmetric with respect to the compositional parts since it divides all parts by the geometric mean. It also has the benefit of being an isometric transformation (Aitchison, 1986). However, the clr transformation has the shortcoming of the transformed data being collinear, since all components add up to 0, and therefore still succumb to the constant sum constraint (Egozcue et al., 2003). Also, this transformation is not appropriate for use in robust PCA since the transformed data do not have full rank, and robust covariance estimators like the MCD estimator need a full rank data matrix (Filzmoser et al., 2009).

The isometric log-ratio (ilr) transformation preserves all the advantageous properties of the clr transformation, solves the collinearity problem, and allows for a robust covariance estimator such as the MCD (Egozcue et al., 2003; Filzmoser et al., 2009). It is based on a choice of an orthonormal basis on the hyperplane (subspace of one dimension less than its ambient space). Since the transformed data are in the hyperplane, there are problems with interpretation as the new D-1 variables have no direct connection to the original variables, being combinations of those variables. To enable interpretation,

Filzmoser et al. (2009) showed how to back-transform the resultant loadings and scores from PCA based on ilr transformed data to the clr space.

Spatial Visualization using GIS

GIS is useful for visualizing spatial data on a map using both the location and characteristics of spatial features. GIS is also a powerful tool for storing, organizing, and managing spatially referenced data linked to other georeferenced datasets. Increasing volumes of geoscience data are being placed into GIS and integrated with other geoscience data. Vector spatial data in the form of points, lines, and polygons, as well as raster data can be overlain, merged, and analyzed through GIS tools and database queries (Chang, 2013; Clemmer, 2013; Grunsky, 2010).

Geochemical spatial variation can be visualized by creating a statistical surface through GIS spatial interpolation. Spatial interpolation approximates the values of the discrete sample points over the whole study region, attempting to recreate the continuous geochemical variation that was discretely sampled in the field. The sample points have known values that are used to estimate values at other points to create a raster statistical surface. This can then be displayed in various ways, such as smooth or contoured. Particularly useful spatial interpolation techniques for geochemical data visualization are trend surface models which are a form of global interpolation, and kriging which is a local interpolation method.

Trend surface models are useful if a smoothed visualization of larger scale trends is desired; this smooths over local variation. A polynomial equation approximates the known points and this equation is used to estimate the unknown areas. Higher order

polynomials are needed to approximate more complex surfaces and involve more computation. Esri's ArcGIS offers up to 12th order trend surface models.

Kriging is an advanced geostatistical procedure that generates an estimated surface from a scattered set of points. Chang (2013) provides a good overview of this technique. Kriging originated as a tool to assist in spatially modeling ore bodies in mining and geologic engineering. Spatial variation is assumed to be neither totally random (stochastic), nor deterministic. This assumption has resulted in different kriging methods being developed. All methods use semivariance or spatial autocorrelation to construct a semivariogram cloud containing all pairs of all points. The semivariogram is fitted with a mathematical function or model, which is then used for estimating the semivariance at a given distance. The next part of the procedure depends on which type of kriging is selected. Three basic kriging methods are: ordinary kriging, universal kriging, and simple kriging. Ordinary kriging is usually the most useful as it focuses on the spatial correlation. Values for unknown points are estimated by solving a set of simultaneous equations based on the fitted semivariogram values for a chosen set of sample points to use. A benefit of kriging is the inclusion of a variance measure (prediction error) for each estimated point that gives an indication of the quality of prediction.

Peninsular Ranges Batholith (PRB), Trends and Previous EDA Work

Northern PRB Subdivisions

The part of the Peninsular Ranges batholith located north of latitude 33˚ N has historically been subdivided in various ways. The most basic subdivision is a batholith-wide separation into eastern and western parts based on criteria such as the

magnetite/ilmenite line, oxygen isotopes and the Sr_i (initial strontium) 0.706 line (Miller et al., 2014; Morton et al., 2014; Ortega-Rivera, 2003; Symons et al., 2003).

Baird et al. (1979) divided the batholith into three post-batholith (Tertiary) structural blocks: the Santa Ana block, the Perris block, and the San Jacinto block. The Elsinore fault zone separates the Santa Ana and Perris blocks, whereas the San Jacinto fault zone separates the Perris and San Jacinto blocks (**Figure 5**). This subdivision is supported by Gromet and Silver (1987), who noted a systematic west/east variation in rare earth element (REE) patterns that suggested a division of the batholith into three distinct parallel longitudinal regions approximately corresponding to Baird's structural blocks.

Morton et al. (2014) created five distinctive longitudinal batholith zones based on field characteristics, geochemistry, age, stable isotopes, and geophysical parameters. The zones are: western zone (WZ), western transition zone (WTZ), eastern transition zone (ETZ), eastern zone (EZ), and upper plate zone (UPZ). The UPZ is allochthonous whereas the other zones are autochthonous. Although the zones are distinct from each other, there is some overlap and gradation between them due to batholith emplacement processes being transitional in nature.

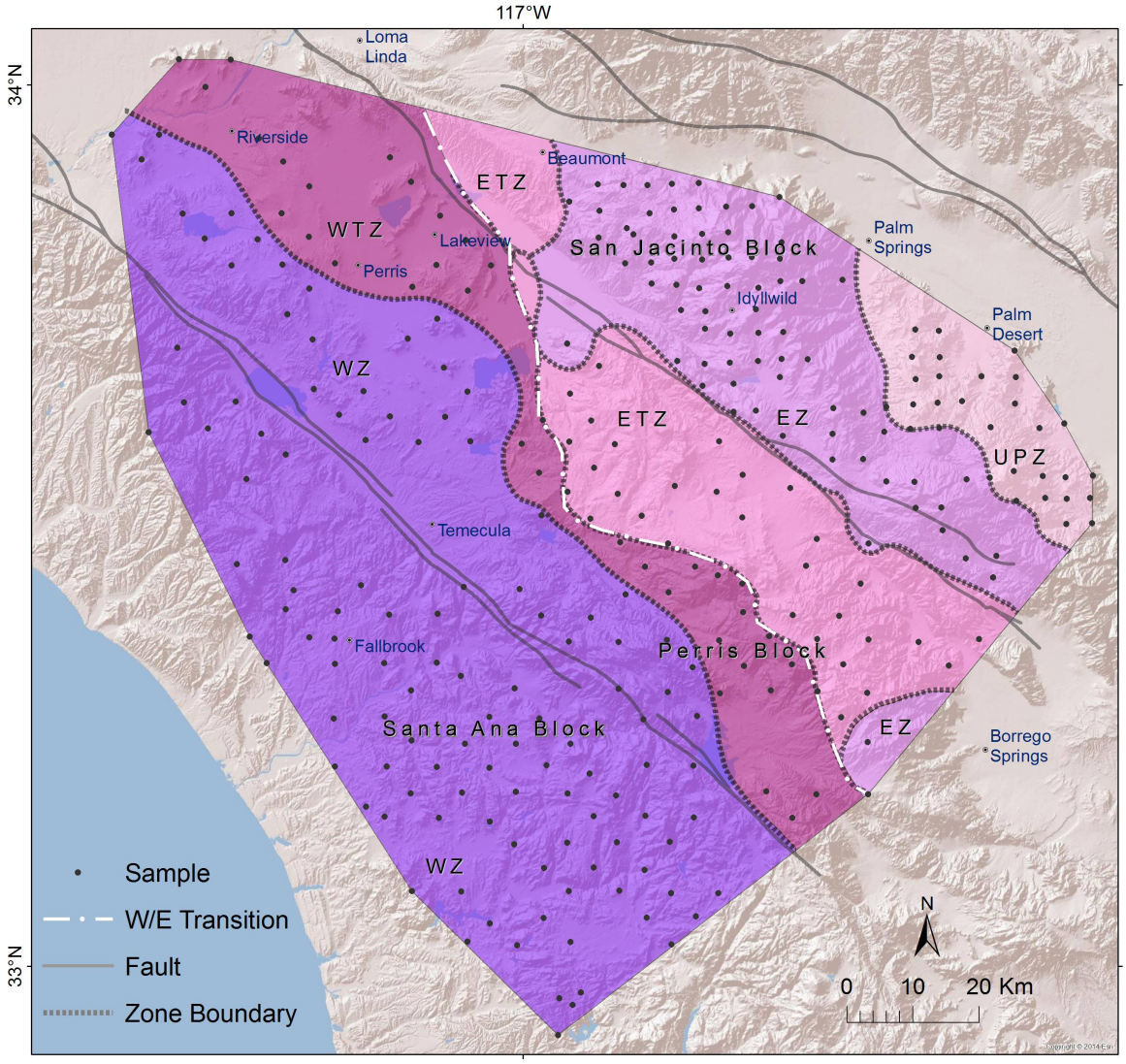

Figure 5. Map of subdivisions of the northern Peninsular Ranges batholith of southern California showing sample locations, structural blocks (Baird and Miesch, 1984) and zones (Morton et al., 2014). A west/east transition zone is placed at the boundary between the WTZ and ETZ to subdivide the batholith into western and eastern parts.

Northern PRB West/East Variation

The northern Peninsular Ranges batholith is laterally zoned, with plutonic rocks differing compositionally between the west and east. The west is more mafic and heterogeneous, and plutons were generally emplaced at a shallower depth than those in the east (Langenheim et al., 2014; Morton et al., 2014). Western rocks are the product of

magmatic activity that formed numerous individual plutons with compositions and internal structures consistent with mixing of granodiorite and gabbro magmas (Clausen et al., 2014). Gabbroic rocks are found mostly southwest of the San Jacinto Fault. The western part of the northern Peninsular Ranges batholith is interpreted to have been emplaced into oceanic crust created from the accretion of an island arc onto an active continental margin, whereas the east is interpreted to have been emplaced into continental crust (Morton et al., 2014).

A distinctive feature of plutons in the east is that they tend to be larger in size than in the west and often display concentric zoning. They are known as "La Posta-type plutons" after the La Posta pluton straddling southern California and Mexico (Clinkenbeard and Walawender, 1989). Walawender et al. (1990) found these plutons to be inwardly zoned from hornblende-bearing tonalite margins to muscovite-bearing monzogranite cores. The San Jacinto mountains in the north-eastern part of the Peninsular Ranges batholith are described by Hill (1984) as having three major tonalite intrusions that he named units I, II, and III. Although they are similar compositionally, being composed of tonalite gradational to K-feldspar-poor granodiorite, they can be differentiated using structural features of a zoned pluton.

Previous Exploratory Data Analysis in the Northern PRB

The use of factor and principal component analysis in batholithic geochemical datasets has been limited to date, but some work has been done using factor analysis in the northern PRB. A few studies have also included geochemical spatial contouring.

Morton et al. (1969) sampled 162 locations over the Lakeview mountains pluton. Computerized trend surface analysis was done at a time that hand contouring was still

common. Surfaces of increasing complexity up to eighth order were computed to contour large-scale patterns that were partly obscured by small-scale heterogeneity in the pluton. The goal was to create a surface that captured the large-scale systematic trends but not the small-scale variability. Systematic concentric zoning was identified with 5^{th} order trend surface analysis showing a mafic core and felsic margin – the inverse of typical zoned plutons.

In a study of spatial trends of major elements over the northern PRB and Transverse Ranges, Baird et al. (1979) used third order trend surface analysis to smooth local noise and create contour maps. They describe a strong SW to NE mafic to felsic gradient, with decreasing Mg, Ca, Fe and density to the NE. They noted that regional chemical gradients, especially for Si and K, varied in a smooth fashion; however at a smaller pluton scale, temporal overlaps interrupt this pattern for parts of the batholith. They also noticed a tendency for the youngest and furthest east rocks in the batholith to be less mafic than earlier rocks.

Baird and Miesch (1984) examined the northern PRB and Transverse Ranges samples using Q-mode factor analysis to create a mixing model for their source materials which suggested 4 possible end members (two magmas and two differentiates) from 8 measured major element oxides (see also Miesch (1976)). Q-mode factor analysis looks at correlations between the samples across a number of variables (sample-based factor analysis), instead of looking at correlations between variables across a number of samples (variable-based factor analysis) which is known as R-mode factor analysis (Klovan, 1975).

CHAPTER TWO

DATA AND METHODS

Northern PRB Dataset

In the mid-1970s, Alex K. Baird and his graduate students Edward Welday and Kathleen White of Pomona College collected regional geochemical and isotope data for the northern PRB and Transverse Ranges. According to Morton et al. (1985), this work culminated in the first accurate assessment of the systematic chemical variation across a composite batholith, and is likely the best dataset in existence for any batholith. They collected the samples on a predesigned grid using a strategy to mitigate the effects of heterogeneity and sampling bias at each sample site. The high quality of the dataset based on these systematically collected samples allows an accurate estimation of the composition of the northern PRB and Transverse Ranges. The Baird-Welday collection includes 480 composite samples collected over an area of 45,000 km^2 with 287 samples falling within the northern PRB and 193 within the Transverse Ranges. Data from these samples include 10 major and 29 trace and rare earth elements (REE), and 4 isotopes and isotope ratios as follows:

- Major elements, analyzed by Baird and Miesch (1984) and Morton et al. (2014): Si, Al, Fe, Mg, Ca, Na, K, Ti, P, Mn.
- Trace elements, analyzed by Morton et al. (2014): Rb, Cs, Sr, Ba, Zr, Hf, Nb, Ta, Th, U, Y, La, Ce, Pr, Nd, Sm, Eu, Gd, Tb, Dy, Ho, Er, Tm, Yb, Sc, V, Cr, Co, Ni.
- Isotopes and isotope ratios (for some samples), analyzed by Kistler (2003), Kistler et al. (2014) and Silver et al. (1988): $^{18/16}O$, $(^{87}Sr/^{86}Sr)_o$, $(^{143}Nd/^{144}Nd)_o$, $(^{206}Pb/^{204}Pb)_o$.

Since this dataset is comprehensive, no additional sampling was needed, however relevant field and lab experience is described in **Appendix 1** and **2**.

Methods

Data Preparation

The PRB geochemical data were first checked for missing values. Although missing data was not a problem, a small number of values were below the detection limit. For P_2O_5, 10 values were below the detection limit of 0.05 ppm, and MgO had six values below the detection limit of 0.1 ppm. Since the number of values below the detection limit was relatively small, censoring was not an issue and they were substituted with values at half the detection limit (Helsel, 1990; Templ et al., 2009). Ni was excluded due to contamination concerns from the milling process.

Since the 10 major oxide values are given in units of weight percent while the 28 trace and rare earth elements are in ppm, standardization was done by representing all values in terms of elemental ppm, excluding the oxygen component from the major elements.

Multivariate and Univariate Assumptions

In the case of compositional data, standard descriptive statistics are not very informative, since the mean, variance, and standard deviation do not fit with the Aitchison geometry as measures of central tendency and dispersion (Pawlowsky-Glahn et al., 2007). As noted, PCA is particularly sensitive to outliers which are commonly handled by detection and removal or by applying a transformation. However, in the case of compositional data, outlier detection is not trivial, making a robust approach preferable

(Filzmoser and Hron, 2008). Spatial interpolation is also sensitive to outliers, requiring their identification and removal. This was done using boxplots.

Principal Component Analysis (PCA)

PCA was run using the R statistical package version 3.2.4 (R-development-core-team, 2016). The "RobCompositions" package (Templ et al., 2016) was used to perform robust PCA for compositional data. This was done using the following steps as implemented in the "pcaCoDa" function:

1. Transform the raw data using the ilr transformation.
2. Perform robust PCA.
3. Back-transform the resulting loadings and scores to clr space.

When displaying PCA results, it is useful to include both the variable loadings and sample scores (known as observations) together on the same plot, called a *biplot*, as first described by Gabriel (1971). To effectively view both the variables and observations at the same time, centering and scaling is done. For the interpretation of biplots for compositional data analysis, see Aitchison and Greenacre (2002) and Pawlowsky-Glahn et al. (2007). Some of the main features important in interpreting biplots are:

- The choice of scale for the loadings and scores.
- Variables are represented as vectors with the length representing the relative strength of the variable's loadings for the principal components plotted.
- Orientation of vectors represents the correlation with respect to other variables and to the observations.
- Vectors oriented close to each other are highly correlated.

- Vectors oriented 180° from each other are negatively correlated.
- Vectors oriented 90° from each other are uncorrelated (orthogonal).
- Observations close to variables are strongly related to them.

In the R implementation of robust compositional PCA, the "pcaCoDa" function creates an object of class "pcaCoDa" which includes an object of the standard PCA routine "princomp." The benefit of having the "princomp" object available is that it can be passed to any R function designed to plot the standard PCA output of this class. With this object, the "ggbiplot" package (Vu, 2016) was used to plot the screeplot as well as biplots for the principal components.

Spatial Variation Plots and Maps

West/east variation plots were created using MS Excel with distance from the transition zone calculated using Esri ArcGIS 10.3 for Desktop (Esri, 2016). Spatial interpolation maps were generated using the kriging and trend surface analysis tools in Esri ArcGIS 10.3 for Desktop. Fault data used is from USGS GIS fault data for California (USGS, 2016). The boundaries of the five PRB zones are from Morton et al. (2014).

Spatial interpolation was restricted to the convex hull of the sample locations to ensure the resulting statistical surface is based as much as possible on the data points and is not an extrapolation outside the area sampled. A convex hull may be visualized as the shape created when a rubber band is stretched around a set of points. For more on convex hulls, see Eddy (1977).

CHAPTER THREE

RESULTS

In this section, the results of the multivariate statistical analysis of the PRB geochemistry are presented first as a series of tables and charts, followed by spatial analysis as a series of charts and maps. Discussions and interpretations are given together with the resulting charts and maps instead of in a separate section to improve readability and clarity. Relevant previous work is considered where appropriate as an aid for the interpretation. These prior studies can often be applied to more than one part of the results due to the similarity that exists when exploring geochemical variation both statistically and spatially.

Geochemical Statistical Variation: Principal Component Analysis

Selecting Principal Components (PC) to Retain

Robust PCA for compositional data was run to determine the underlying structure for the 38 geochemical variables for the samples from the northern PRB. Two criteria were used to evaluate the appropriate number of components to retain: eigenvalues and scree plot (**Figure 6**). Examining the eigenvalues and scree plot indicated that retaining two and possibly three components should be investigated. The first principal component (PC1) accounted for 56.7% of the total variance, the second (PC2) 17.3%, and the third (PC3) 6.7%. Therefore, PC1 is more than three times as significant as PC2, while PC2 is almost three times as significant as PC3. **Table 1** gives the variable loadings sorted from low to high for the first three principal components. **Table 2** gives the variable loadings sorted by absolute value for the first three principal components to show the relative

significance of each variable in each principal component. The most significant variables are highlighted for each principal component.

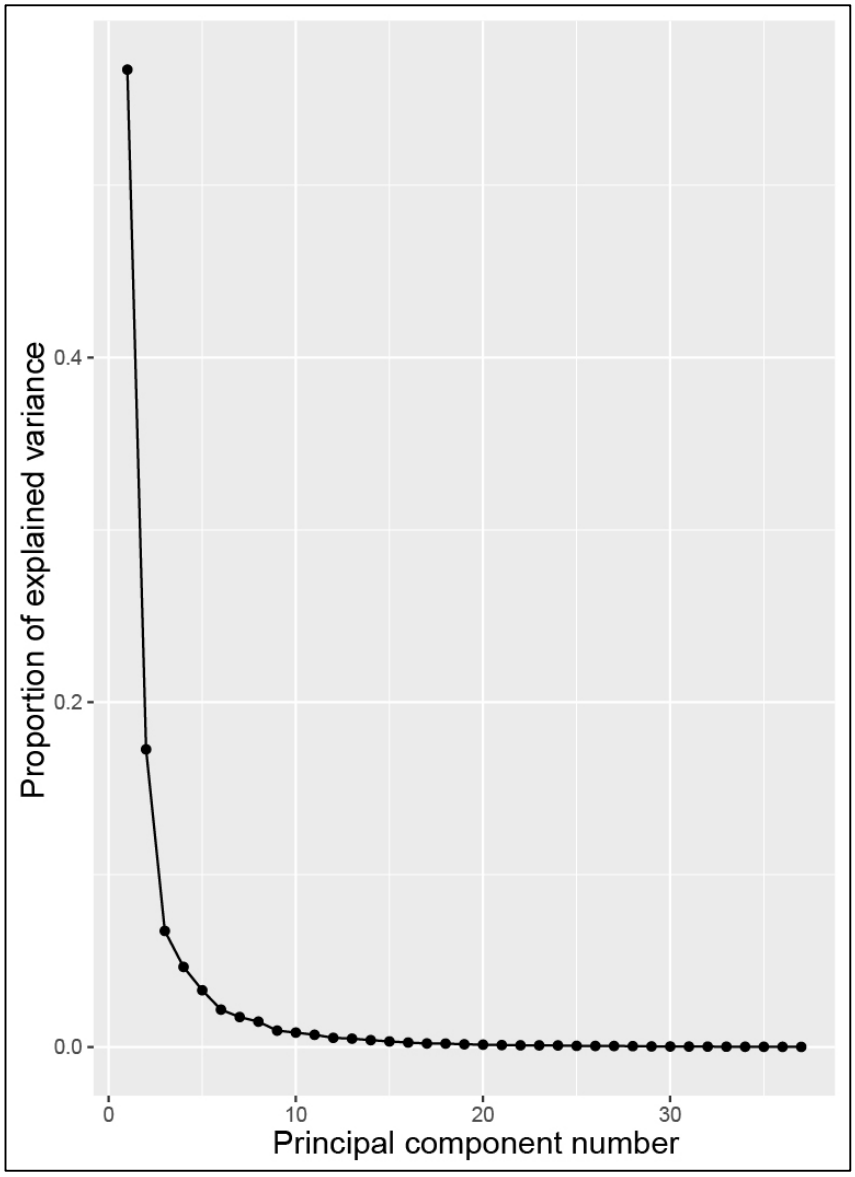

Figure 6. Scree plot for robust compositional PCA suggests retaining two or possibly three principal components.

Table 1. Variable loadings for PC1, PC2 and PC3, ordered from low to high.

PC1	
Th	-0.27
La	-0.22
Ta	-0.22
Ce	-0.21
Nb	-0.19
Rb	-0.19
Ba	-0.18
Pr	-0.18
U	-0.17
K	-0.16
Nd	-0.14
Zr	-0.11
Hf	-0.10
Sm	-0.08
Cs	-0.08
Sr	-0.05
Eu	-0.02
Gd	-0.01
Si	0.00
P	0.00
Na	0.00
Tb	0.02
Al	0.05
Dy	0.06
Ho	0.07
Y	0.09
Ti	0.09
Er	0.10
Tm	0.10
Yb	0.11
Ca	0.16
Fe	0.17
Mn	0.19
Cr	0.25
Mg	0.26
Co	0.27
V	0.30
Sc	0.31

PC2	
Yb	-0.34
Tm	-0.33
Er	-0.28
Ho	-0.25
Y	-0.21
Dy	-0.20
Tb	-0.16
U	-0.13
Cs	-0.13
Th	-0.12
Gd	-0.09
Cr	-0.07
Rb	-0.06
K	-0.06
Hf	-0.05
Sm	-0.01
Sc	-0.01
Zr	0.01
Si	0.03
Mn	0.03
Ta	0.03
Na	0.05
Nd	0.06
Eu	0.08
Pr	0.08
Ce	0.08
Ba	0.08
La	0.10
Al	0.11
Fe	0.12
V	0.12
Co	0.12
Nb	0.14
Mg	0.21
Ca	0.21
P	0.23
Ti	0.24
Sr	0.37

PC3	
Cr	-0.49
Th	-0.41
Cs	-0.39
Rb	-0.23
U	-0.21
Mg	-0.14
V	-0.13
Co	-0.11
Sc	-0.08
La	-0.08
K	-0.08
Ce	-0.04
Pr	0.01
Fe	0.01
Mn	0.03
Zr	0.03
Ca	0.04
Ti	0.04
Hf	0.04
Nd	0.05
P	0.07
Si	0.07
Al	0.08
Nb	0.09
Sm	0.10
Ba	0.11
Er	0.11
Gd	0.11
Yb	0.11
Y	0.12
Ta	0.12
Dy	0.13
Na	0.13
Sr	0.14
Eu	0.14
Ho	0.16
Tb	0.16
Tm	0.18

Table 2. Variable loadings for PC1, PC2 and PC3, ordered by absolute value with more significant values highlighted. Values are in clr coordinate space.

	PC1	PC2	PC3
Sc	0.31	-0.01	-0.08
V	0.30	0.12	-0.13
Th	-0.27	-0.12	-0.41
Co	0.27	0.12	-0.11
Mg	0.26	0.21	-0.14
Cr	0.25	-0.07	-0.49
La	-0.22	0.10	-0.08
Ta	-0.22	0.03	0.12
Ce	-0.21	0.08	-0.04
Nb	-0.19	0.14	0.09
Mn	0.19	0.03	0.03
Rb	-0.19	-0.06	-0.23
Ba	-0.18	0.08	0.11
Pr	-0.18	0.08	0.01
U	-0.17	-0.13	-0.21
Fe	0.17	0.12	0.01
K	-0.16	-0.06	-0.08
Ca	0.16	0.21	0.04
Nd	-0.14	0.06	0.05
Zr	-0.11	0.01	0.03
Sr	-0.05	0.37	0.14
Yb	0.11	-0.34	0.11
Tm	0.10	-0.33	0.18
Er	0.10	-0.28	0.11
Ho	0.07	-0.25	0.16
Ti	0.09	0.24	0.04
P	0.00	0.23	0.07
Y	0.09	-0.21	0.12
Dy	0.06	-0.20	0.13
Cs	-0.08	-0.13	-0.39
Tb	0.02	-0.16	0.16
Eu	-0.02	0.08	0.14
Na	0.00	0.05	0.13
Gd	-0.01	-0.09	0.11
Sm	-0.08	-0.01	0.10
Al	0.05	0.11	0.08
Si	0.00	0.03	0.07
Hf	-0.10	-0.05	0.04

Biplot of PC1 vs. PC2

Geochemical variables and samples (also called observations) are visualized together in a biplot for the first and second principal components with the samples grouped by lithology **(Figure 7**) as well as by PRB structural block (**Figure 8**). Ellipses capture one standard deviation of the variation in each group (68.27%).

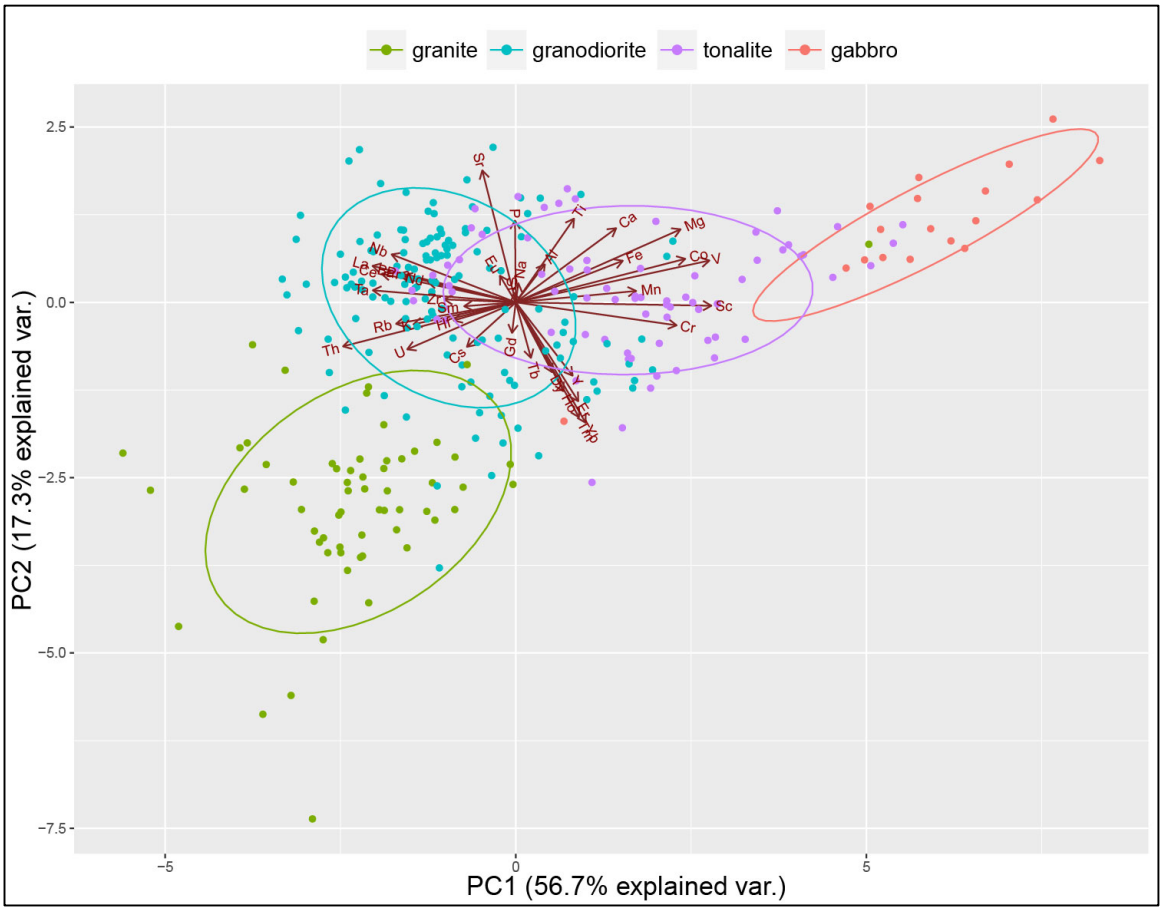

Figure 7. PC biplot of PC2 vs. PC1 with samples grouped by rock type. After performing robust PCA of ilr-transformed data, the resulting PC1 and PC2 variable loadings as well as sample scores were back-transformed to clr space for biplot representation. Variables are represented by vectors and samples by points classified by rock type. Ellipses depict one standard deviation of rock type distribution. A monotonic trend from mafic (high PC1) to felsic (low PC1) is seen.

For the samples in **Figure 7**, the most noticeable effect is a monotonic trend from mafic to felsic, with gabbros at high PC1 transitioning through tonalite, granodiorite and granite at low PC1. Both the gabbro and granite groups minimally overlap in 2-D space with their closest neighbors (tonalite and granodiorite respectively) while the intermediate groups of tonalite and granodiorite overlap more extensively with each other. However when considering only PC1, only gabbro does not overlap with its neighbors considerably. This mafic to felsic trend is reflected most strongly in PC1, which explains 56.7% of the total variation.

Grouping the samples by PRB block (**Figure 8**) reveals a weak trend explained mainly by PC2. The three block subdivisions are used instead of the five zone subdivisions in order to visualize general west/east trends without too much detail being presented in biplots and to facilitate comparison with previous studies. The western Santa Ana block samples, central Perris block samples and eastern San Jacinto block samples are oriented in a general west/east trend with some overlap.

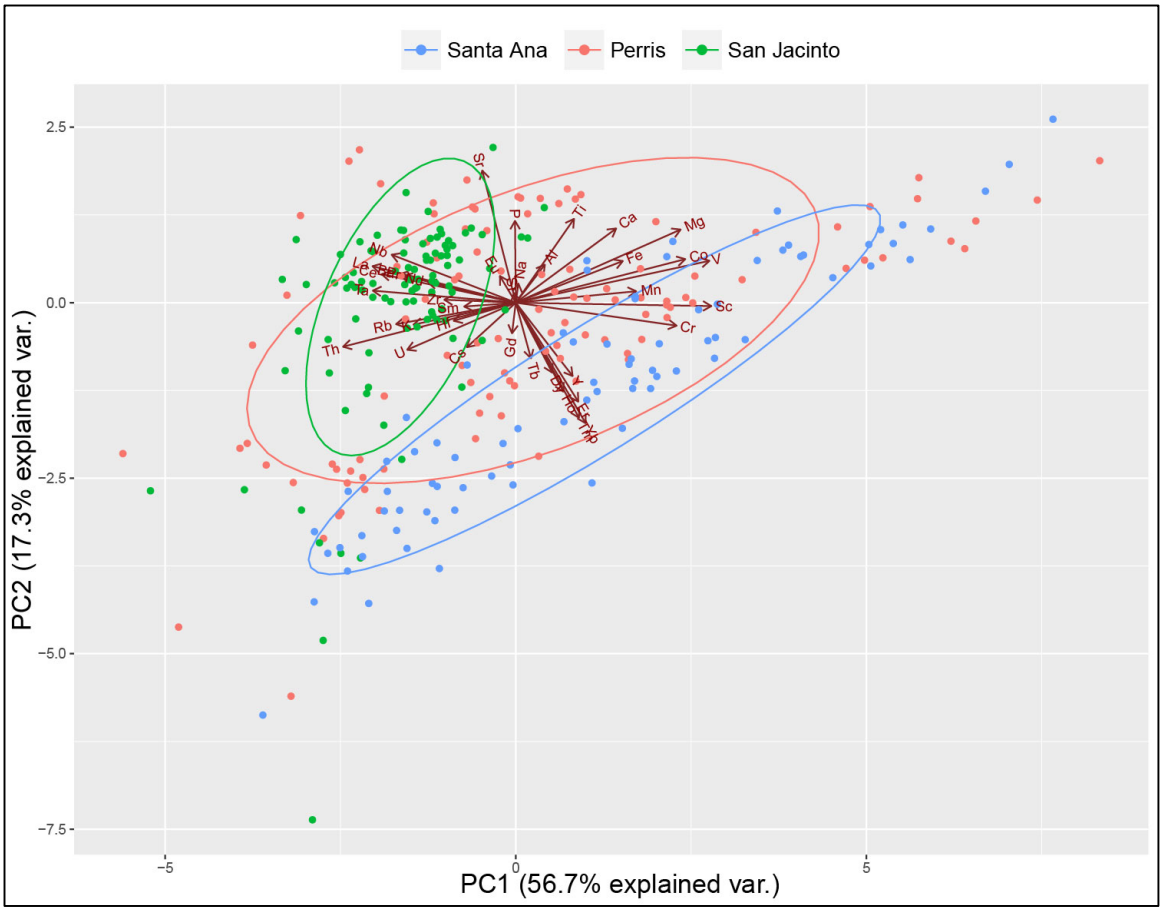

Figure 8. PC biplot of PC2 vs. PC1 with samples grouped by PRB block. After performing robust PCA of ilr-transformed data, the resulting PC1 and PC2 variable loadings as well as sample scores were back-transformed to clr space for biplot representation. Variables are represented by vectors and samples by points classified by rock type. Ellipses depict one standard deviation of PRB block distribution. A weak monotonic predominantly PC2 trend from the Santa Ana block to the San Jacinto block is seen.

The vectors representing geochemical variables show similar trends, with compatible elements at high PC1 (Ti, Ca, Mg, Fe, Co, V, Mn, Sc, Cr) found in greater abundance in mafic minerals oriented toward higher PC1 and the mafic gabbro samples (see **Figure 7** and **Figure 9** for a zoomed view of the variables). The compatible elements consist mainly of the transition elements in **Figure 3**. They are not tightly clustered, varying with respect to each other in terms of PC1 and PC2. Most other elements display

incompatible behavior to varying degrees (low PC1), with strongly incompatible elements (Rb, K, Th, U, Cs) found in the opposite direction from the compatible elements, showing a negative correlation.

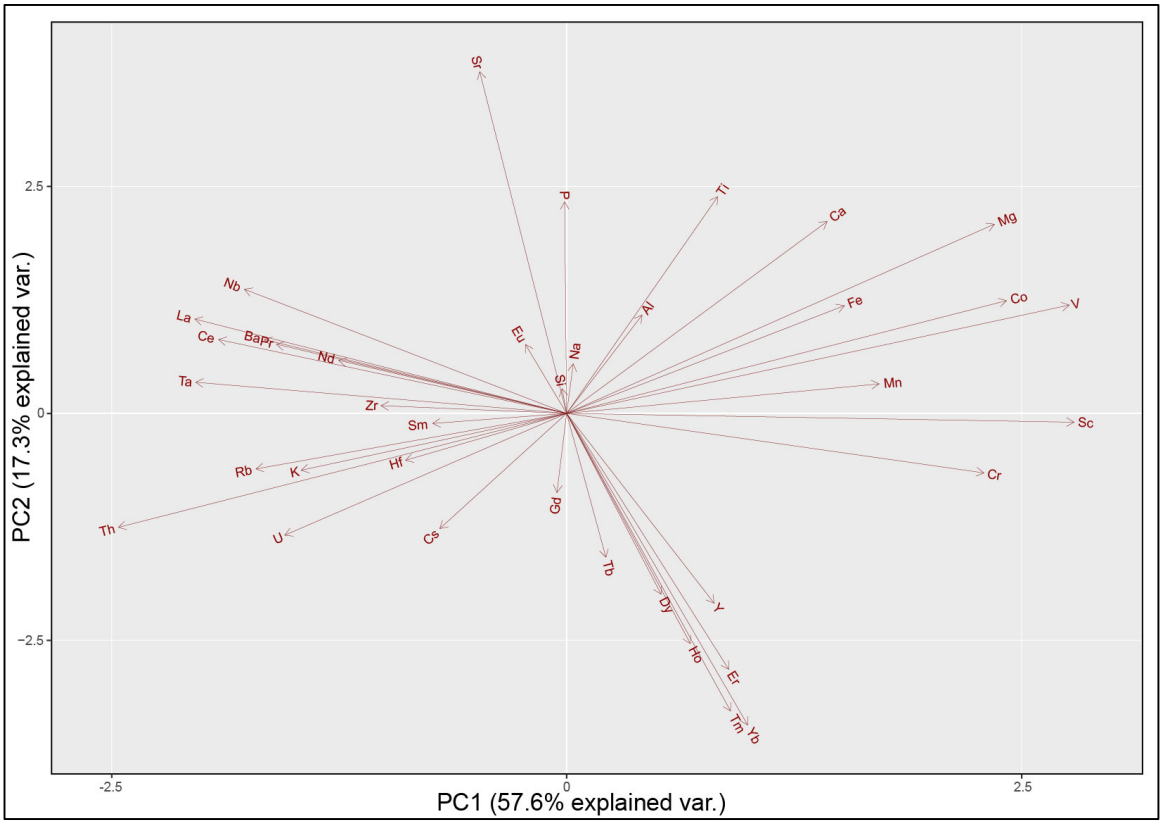

Figure 9. PC biplot of PC2 vs. PC1 – zoomed view of variables.

Although Si comprises a higher ratio of the composition of samples than any other element (42-76 wt. %), it is close to zero in the biplot, being slightly positive in PC2. This is because it occurs in both shallow and deep, and felsic and mafic samples and shows relatively low variation among samples when compared to the other elements.

Order of Incompatibility

According to Sun and McDonough (1989), the order of incompatibility of trace elements in mid-ocean ridge basalts (MORBs) and ocean island basalts (OIB) follows the sequence: Cs ≈ Rb ≈ Ba > Th > U ≈ Nb = Ta ≈ K > La > Ce > Pr ≈ Mo ≈ Sr > P ≈ Nd > Zr = Hf ≈ Sm > Eu ≈ Ti > Dy ≈ Li > Ho = Y > Yb. They state that the rule works in general, suggesting relatively simple overall fractionation processes of partial melting and fractional crystallization (PM/FC) and no significant change in the environment of formation of MORBs and OIBs.

The variable loadings for PC1 (see **Table 1**) suggest that the order of incompatibility for the PRB samples, and by implication for felsic crustal rocks, is as follows: Th > La = Ta ≈ Ce > Nb = Rb ≈ Ba = Pr ≈ U ≈ K > Nd > Zr > Hf > Sm = Cs > Sr > Eu ≈ Gd ≈ Si = P = Na > Tb> Al ≈ Dy ≈ Ho > Y = Ti ≈ Er = Tm ≈ Yb > Ca ≈ Fe > Mn > Cr ≈ Mg ≈ Co > V ≈ Sc. This ordering is a progression from the most incompatible element (Th) to the most compatible (Sc).

The variables and samples both suggest an interpretation for PC1 of **extent of differentiation**, a result of cycles of partial melting and fractional crystallization. This principal component is also related to **crustal contamination** of magma (and therefore to initial strontium), since elements that are more compatible remain in the mantle while incompatible elements migrate into the crust.

Depth effect of Garnet and Plagioclase

The heavy rare earth elements, Tb, Dy, Ho, Er, Tm, Yb as well as Y are clustered and oriented along the PC2 trend and toward the western Santa Ana block samples in

Figure 8. Several LREEs (La, Pr, Nd, Sm) are clustered toward low PC1, oriented mainly along PC1 and towards the eastern San Jacinto block. In the plot of ionic radius vs. ionic charge (**Figure 3**) the rare earth elements are grouped closely together, suggesting similar behavior is expected in the way they fit into a crystal lattice and substitute for other elements.

Garnet is a major high pressure rock-forming mineral, is stable and could be volumetrically important across a broad range of compositions at high pressure (Gromet and Silver, 1987). It is abundant in the deeper garnet stability zone (> 33-40 km depth), occurring for example in eclogite and high pressure garnet amphiboles (Otamendi et al., 2002). As noted earlier, garnet acts as a sink for the heavy and middle REEs as well as for Y, causing fractionation. Recall from **Figure 4** the partition coefficients of the heaviest REEs are about three orders of magnitude greater than for the lightest REEs, so at the depth of the garnet stability zone, concentrations of HREEs in garnet crystals are about one thousand times greater than LREE concentrations. Similarly, HREEs in the melt derived from garnet fractionation will be about one thousand times lower in abundance than LREEs (Morton et al., 2014).

A melt derived from the shallower depth plagioclase stability zone (< ~10 km depth), where garnet is not stable, will not show the depletion in heavy REEs. However, crystallization of plagioclase at this level depletes the melt of Sr and Eu. Feldspars are the only major rock unit capable of storing Sr (Gromet and Silver, 1987). Although plagioclase and garnet are not the only minerals crystalizing at their respective depths, they are volumetrically important enough to dominate the behavior of the REE, Sr and Y.

Figure 10 shows clusters of elements that are relatively depleted in near surface granitoids due to removal by garnet and plagioclase differentiation at depth. The near surface granitoids are a complement of the deeper more mafic rocks containing garnet and higher plagioclase. The alkali elements are enriched in these final stage high K-feldspar granitoids.

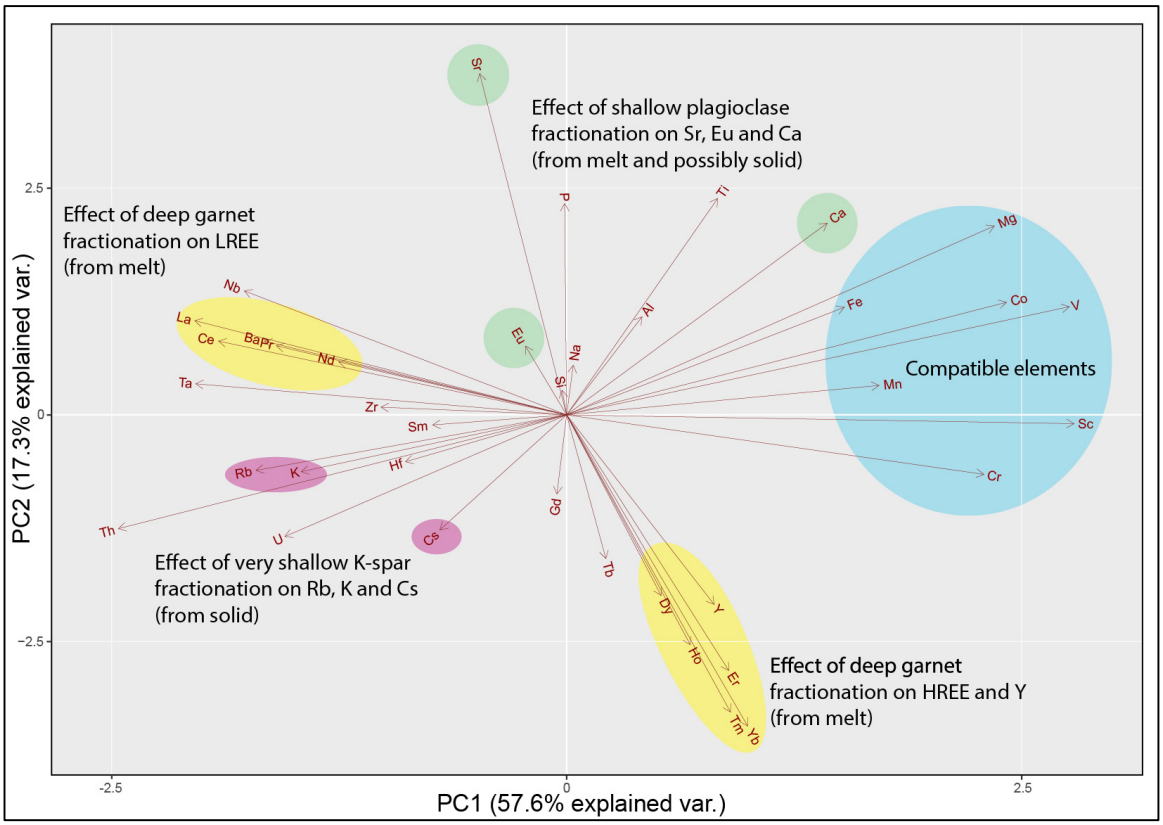

Figure 10: PC Biplot of PC2 vs. PC1 showing the effect of deep garnet differentiation on HREE, Y and possibly LREE and the effect of intermediate level plagioclase differentiation on Sr, Eu and Ca. K-feldspar influences K, Rb and Cs close to the surface. Compatible elements are clustered at high PC1. The LREE are affected more by PC1 than by PC2, indicating differentiation extent.

Thus, PC2 is similar to the standard geochemical parameter Sr/Y as a measure of magma source depth, but it includes more elements that are partitioned in a similar

manner by the effect of pressure and therefore depth. These relationships suggest that a reasonable interpretation for PC2 would be **magma source depth**.

Looking at the fractionating effect of garnet in more detail, a direct relationship between the order of PC2 loadings and ionic size for the REEs is seen. In order of increasing ionic size and PC2 loading, the sequence is: Yb, Tm, Er, Ho, Dy, Tb, Gd, Sm, Nd, Pr, Ce and La. In **Figure 11**, red arrows show the direction of increasing concentration for the solid and melt phases. Elements with larger ionic radii tend to be partitioned more into the melt since they do not fit well into the solid crystal lattice – an effect which increases as pressure increases. This observation indicates that the upper crust PRB granitoids come from melt depleted in garnet and plagioclase elements that have been fractionated out in the mantle and lower crust, but enriched in the K-feldspar elements that remained after emplacement into the upper crust. Since K-feldspar is stable close to the surface, its effect is likely to be due to sampling the solid. Elements related to garnet, plagioclase, K-feldspar fractionation as well as the most compatible elements are similarly highlighted for comparison between **Figures 10** and **11**.

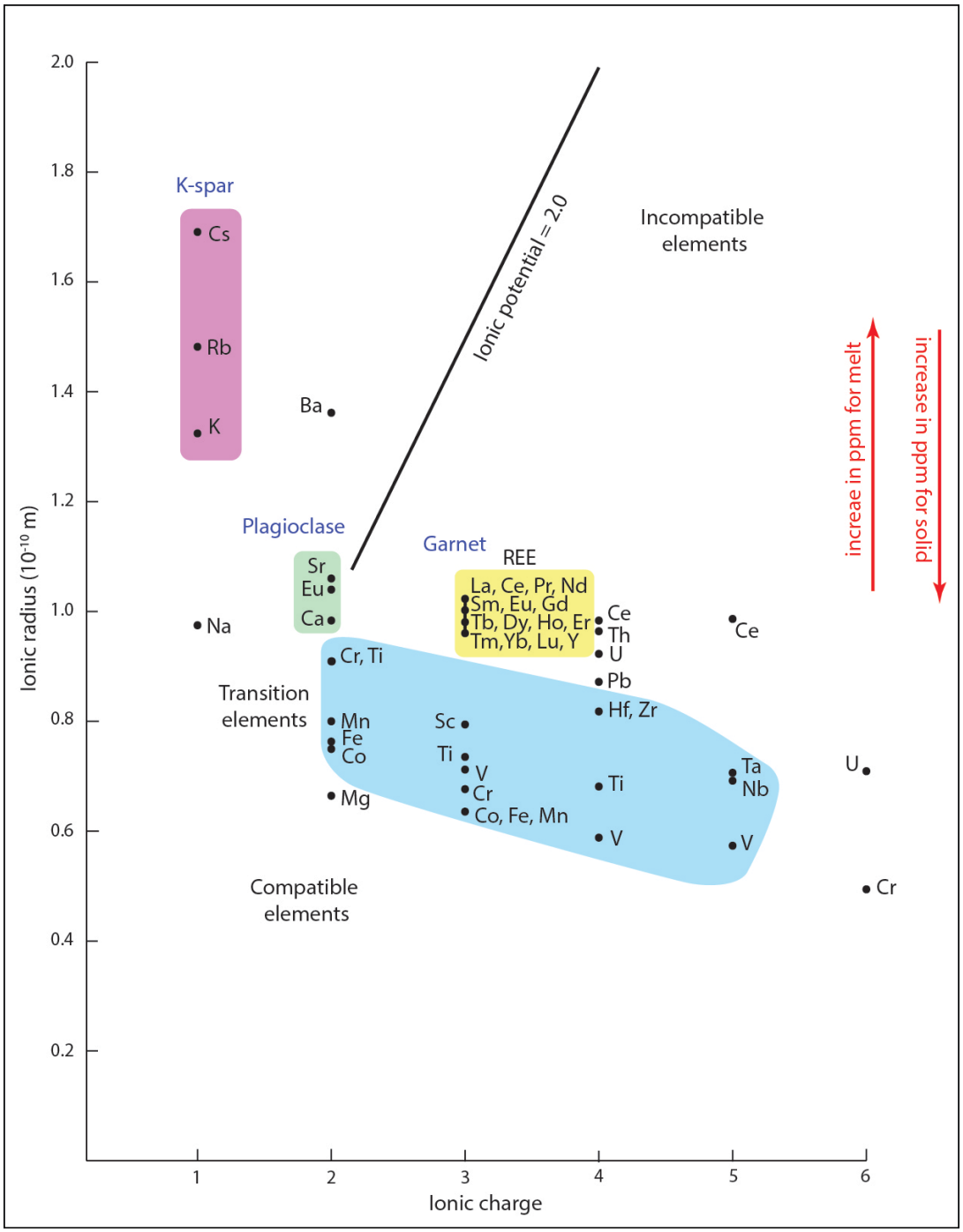

Figure 11: Plot of ionic radius vs. ionic charge with arrows showing direction of increase in abundance of elements with respect to the melt and solid phases. Elements fractionated by garnet, plagioclase and K-feldspar are highlighted. The transition elements tend to be more compatible.

A systematic west/east variation in REE patterns led Gromet and Silver (1987) to divide the batholith into three distinct parallel longitudinal regions, which would roughly correspond to Baird's three structural blocks in **Figure 8**. They proposed a deepening magma source trend to the east with western source rock dominated by a plagioclase-bearing (gabbroic) assemblage while the source rock in the east is dominated by a garnet-bearing plagioclase poor (eclogitic or garnet amphibolitic) assemblage. This idea was supported by observing a strong enrichment in LREEs in rocks in the east, implying a garnet-rich source; and higher Sr in central and eastern rocks, reflecting lower abundance of plagioclase in the source rock. The appearance of garnet and disappearance of plagioclase in sources of the central region were said to be complementary – both are needed to explain REE and Sr patterns.

The west/central transition is correlated with a change in the emplacement style of the batholith from a stationary oceanic island arc in the west to an eastward-migrating arc. The change in REE patterns is attributed to the partial melting of a mafic source to produce a plagioclase-rich gabbro residue at shallow depth in the west, rapidly changing to a deeper, higher-pressure partial melting process producing a garnet-bearing residue in the central and eastern regions. Gromet and Silver (1987) note that the REE geochemistry in the west is consistent with that of an ocean island arc basement, whereas in the central and eastern region, the strong heavy REE fractionation is evidence that it is from a deeper source, possibly due to a basaltic underplate thickening of the continental crust. The west-east contrast is visualized in **Figure 12**. A steep slope indicates a large difference in partition coefficients between the light and heavy REEs, and is interpreted to be the result of garnet fractionation at depth, as evidenced in the eastern San Jacinto block. The

western region of the PRB in the Santa Ana block is characterized by rocks having a more gentle REE slope indicating little effect from garnet fractionation. The REE fractionation pattern in the central Perris region is intermediate between the other two regions.

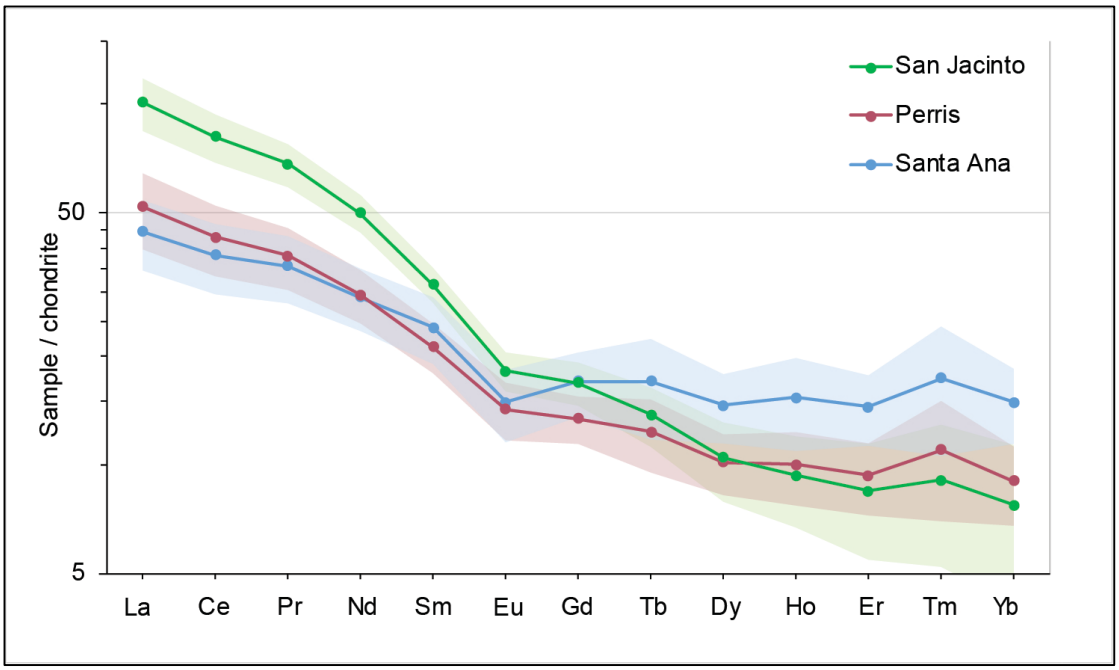

Figure 12. Rare earth multi-element spider diagram for the Santa Ana, Perris, and San Jacinto blocks. REE data are from the 287 samples collected by Baird and Miesch (1984) and analyzed by Morton et al. (2014). Lines represent mean values for all samples, shaded areas represent one standard deviation.

PCA analysis has shown the variation of elements relating to fractionation of garnet and plagioclase can be explained by considering the effect of pressure (and depth). If PC2 relates to magma source depth, it can be used as a geobarometer, reflecting the average depth at which magma originated.

Biplot of PC2 vs. PC3

When the influence of PC1 is removed, the impact of PC2 on the variables and samples is more clearly seen (**Figure 13**). Grouping by rock type, the trend from mafic to felsic reflects the fact that western granitoids from a shallower source are more mafic and eastern granitoids from a deeper source are more felsic, with the most overlap occurring between the intermediate tonalite and granodiorite.

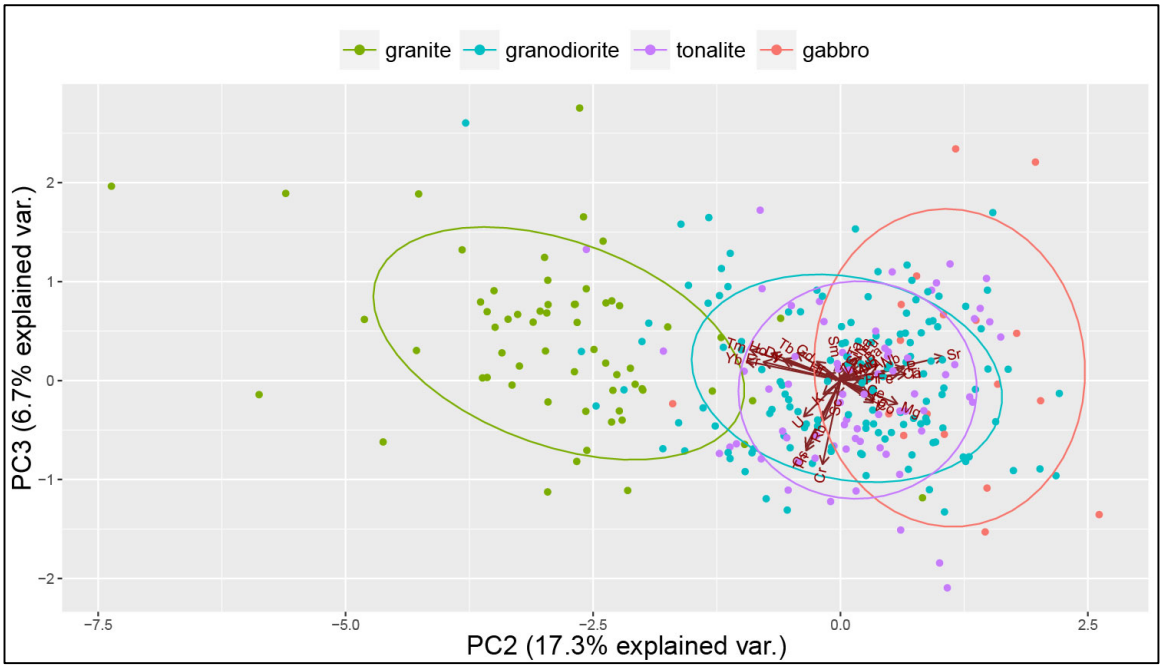

Figure 13. PC biplot of PC3 vs. PC2 with samples grouped by rock type.

When grouping by PRB block, a very weak west/east trend is noticed (**Figure 14**).

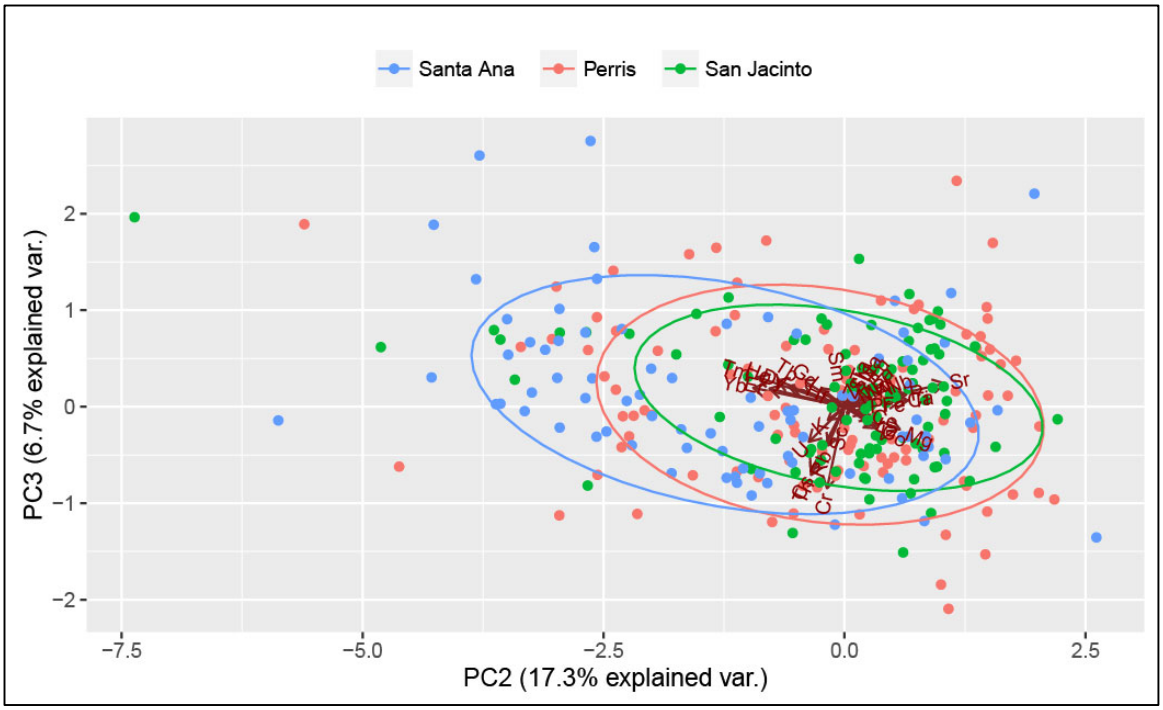

Figure 14. PC biplot of PC3 vs. PC2 with samples grouped by PRB block.

Since PC3 represents only 6.7% of the total variation, an interpretation is not likely to be very meaningful. However, examining the effect of PC3 on the variables in the zoomed view of the biplot of PC2 and PC3 (**Figure 15**), a grouping of elements (K, Sc, Cr, Th, Rb, Cs, U) is noticed oriented toward negative PC3 that have highly water-soluble forms. Nb and Ta, known to be water insoluble are oriented toward positive PC3. The alkali metals are known to be particularly water-soluble, represented here by K, Rb, and Cs. Uranium is water soluble in the form of many of its salts (U^{6+}). Scandium is highly soluble in the form of scandium chloride and other salts. Thorium is mobile in water. Chromium (VI) is highly water soluble (Greenwood and Earnshaw, 2012; Hobbs and Edwards, 1994; James, 1996). Water-soluble elements tend to be more mobile and an increase in the concentration of these elements in rocks could be an indication of the involvement of slab fluids. Higher alkalinity is associated with distance from the trench

as noted by Tatsumi and Eggins (1995). As the subducting slab moves through progressively deeper zones, dehydration melting occurs and water is driven off, carrying water-soluble elements as it ascends with the melt.

A tentative interpretation for PC3 would therefore be solubility and mobility associated with **alkaline** variation. However as noted, PC3 only accounts for 6.7% of explained variance, so a mix of several processes is likely being represented here.

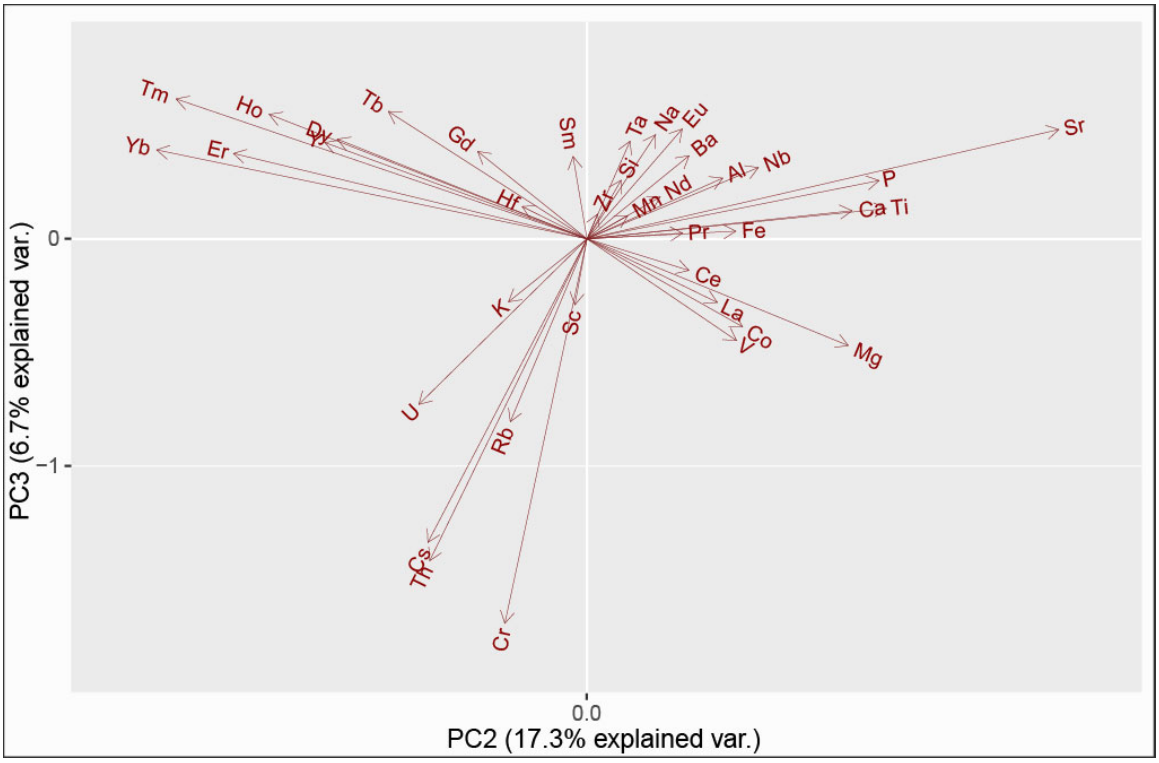

Figure 15. PC biplot of PC3 vs. PC2 – zoomed view of variables.

Geochemical Spatial Variation: Distance Plots and Interpolation Maps

Understanding the spatial distribution of geochemical patterns (the spatial domain) is a fundamental part of geochemical exploratory data analysis. Visualization of spatial variation aids in data interpretation and subsequent model building. First, the

standard geochemical parameters for extent of differentiation, magma source depth, crustal contamination and alkalinity are considered in terms of one-dimensional west/east variation across the northern Peninsular Ranges batholith and then in two-dimensions using spatial interpolation. Second, the principal components are spatially interpolated and compared to the standard geochemical parameters.

West/East Variation (1-D)

Mesozoic magmatism is interpreted to have progressed from west to east in the PRB, traversing a basement of oceanic crust in the west to continental crust in the east (Morton et al., 2014). Between the western and eastern zones, the western and eastern transitional zones are thought to reflect a transition from oceanic to continental crust. An understanding of the shift in geochemical patterns from west to east can shed new light on subduction-zone processes of interest. The five zones of Morton et al. (2014) are compared using bivariate diagrams of standard geochemical parameters associated with subduction zone processes plotted against the distance from the line dividing the western and eastern transition zones. Distance from transition zone was measured as the closest distance from each sample location to the transition zone line, found using GIS. This gives a 1-D or first order variation view of patterns.

For SiO_2 (**Figure 16**) the main difference between the west and east is the degree of variation, with a sharp change being observed across the transition zone. West of the transition zone, SiO_2 varies widely and evenly, especially in the western zone. This is due to the wide range of rocks found in the west, from gabbros to granites. In the east, SiO_2 is confined mainly to the more felsic values and is uniformly high except for a few gabbro samples in the eastern transition zone. The western granitoids are interpreted to have been

emplaced in an extensional plate tectonic regime with a shallow source (Morton et al., 2014). This would allow for relatively fast magma ascent and less time for mixing between mafic and felsic magmas.

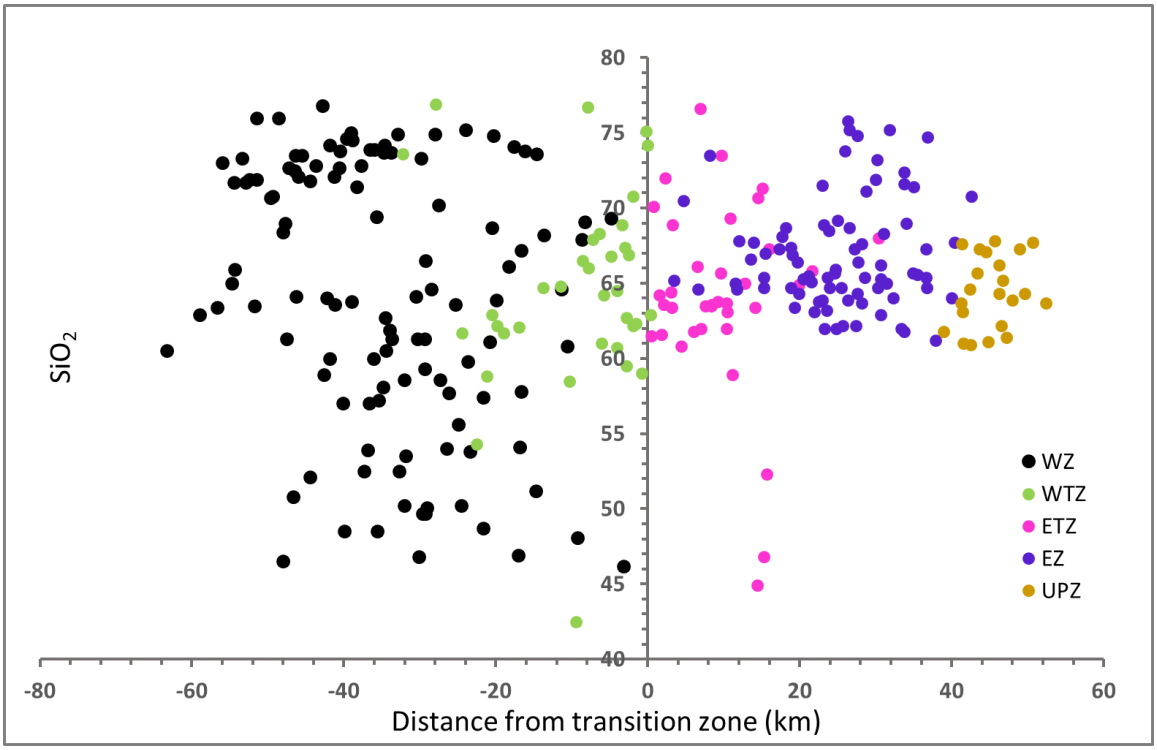

Figure 16. SiO_2 concentration (wt. %) vs. W-E distance from the transition zone dividing line, with samples grouped by PRB zone (WZ - western zone, WTZ – western transition zone, ETZ – eastern transition zone, EZ – eastern zone, UPZ – upper plate zone). The west is characterized by wide variation while the east is high and less variable.

As subduction moved through the transition zone continent-ward, the extensional tectonic regime rapidly changed to a compressional tectonic regime and a deeper source (Gromet and Silver, 1987; Morton et al., 2014). This slowed the magma ascent rate, allowing more time for mixing between magmas with extreme compositions.

Similar to SiO_2, a sharp distinction is noticed between the east and west for initial strontium (**Figure 17**). West of the transition zone, Sr_i shows a slightly increasing trend

with little variation while in the east the degree of variation is greater and a strongly increasing trend is observed, with the highest average values in the transition and upper plate zone.

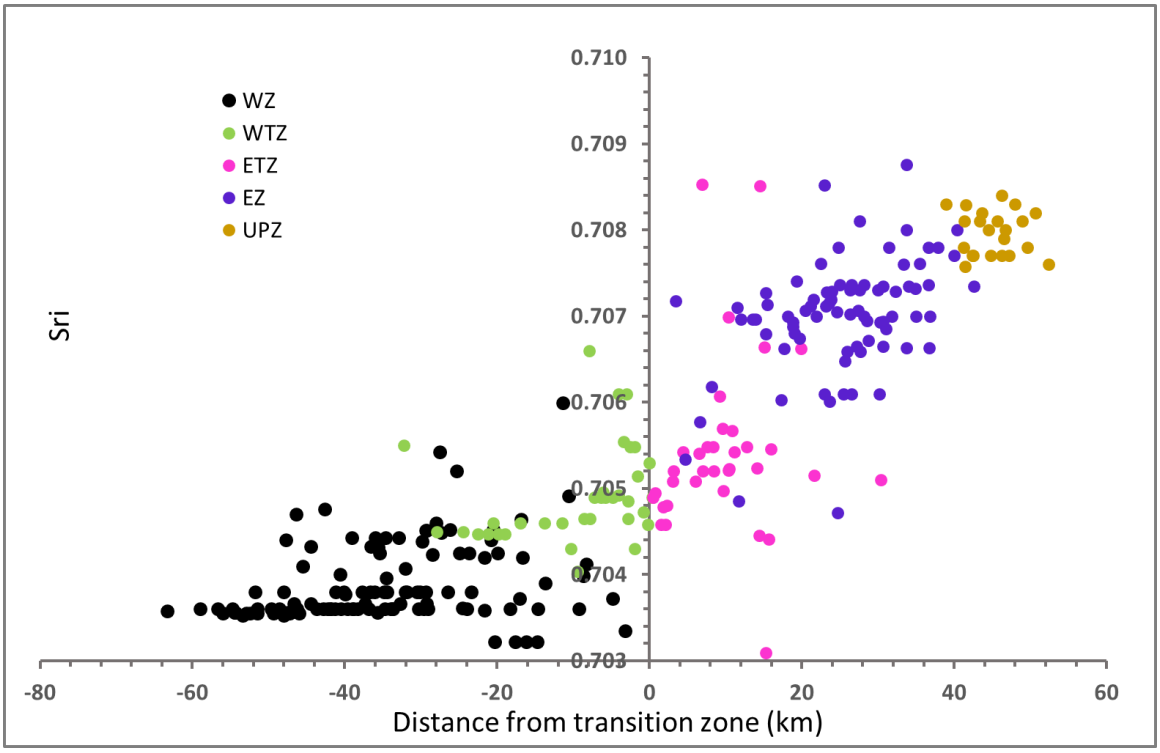

Figure 17. Initial strontium (Sr_i) vs. W-E distance from the transition zone dividing line with samples grouped by PRB zone. In the west Sr_i is low, while in the east it is higher and increases eastward.

If Sr_i records the amount of continental crust contamination, a picture emerges of magmatism proceeding through different basements. Initially magma ascended through oceanic crust in the west with relatively uniformly low contamination, (or high contamination with low Sr_i crust), increasing slightly as the continental influence increases to the east. As subduction moved under the North American craton, crustal contamination rapidly increased. This coincides with a transition from an extensional to a compressional tectonic environment, slowing magma ascent rates. Magma movement is

more constrained, allowing more time for interaction with the continental crust, resulting in a higher degree of crustal assimilation.

The Sr/Y ratio shows an increasing trend from west to east (**Figure 18**). The west has relatively low Sr/Y ratios with little variation while the samples east of the transition zone are more widely dispersed and higher overall. This trend shows source depth to be increasing to the east, with a relatively uniform shallow source in the west and a more variable deeper source in the east. As subduction advanced eastward from where the magma source was in the shallow plagioclase stability zone where strontium was left behind at depth, it encountered the thick continental crust. The increased depth and pressure pushed partial melting into the garnet stability zone, removing yttrium (and HREE) from the melt, but not lowering strontium concentrations from plagioclase fractionation at depth. The greater variation in the east helps to explain the weak trend seen in PRB blocks in **Figures 8** and **14**. Since Sr/Y values are both low and high in the central Perris and eastern San Jacinto blocks, there is a lot of overlap with each other and with the western Santa Ana block.

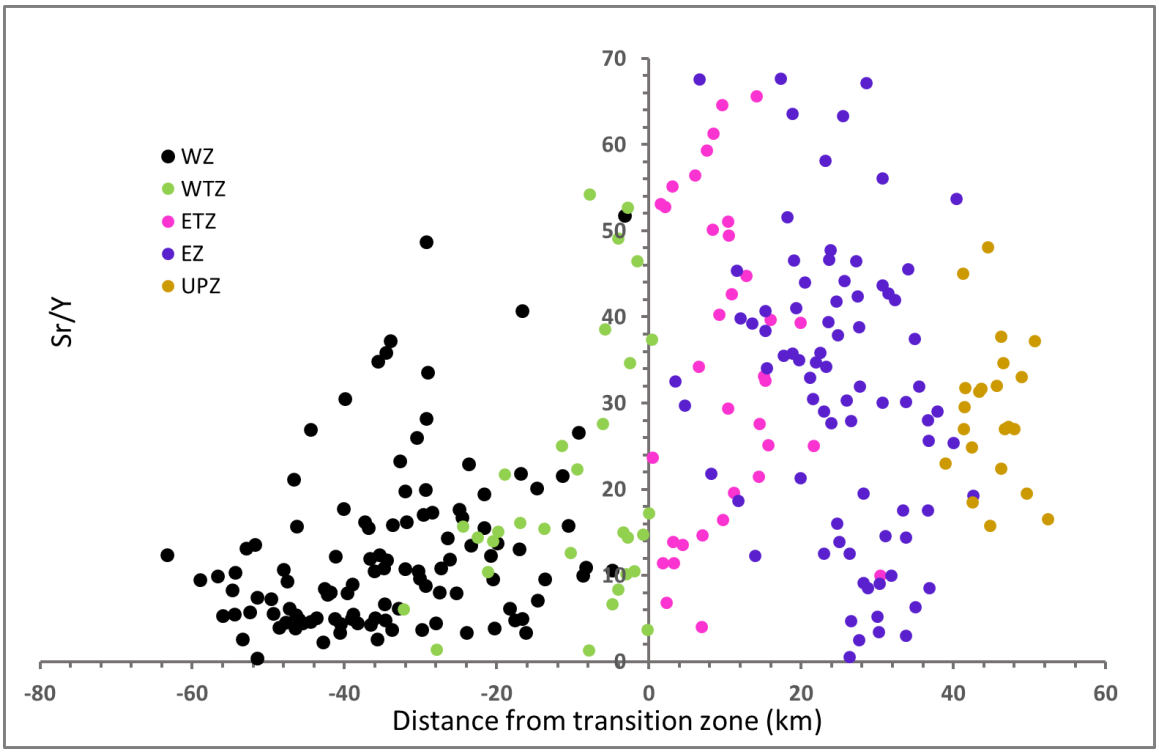

Figure 18. Sr/Y vs. W-E distance from the transition zone dividing line with samples grouped by PRB zone. The west shows a trend of Sr/Y increasing in value and becoming more variable while the east is higher and more variable.

The K_2O/SiO_2 ratio has a dispersed pattern in the west with a less dispersed increasing trend seen in the east (**Figure 19**). As distance east of the trench increases inboard of the subducting slab, an increase in K_2O is seen, as predicted by the K-h relationship of Kuno (1959).

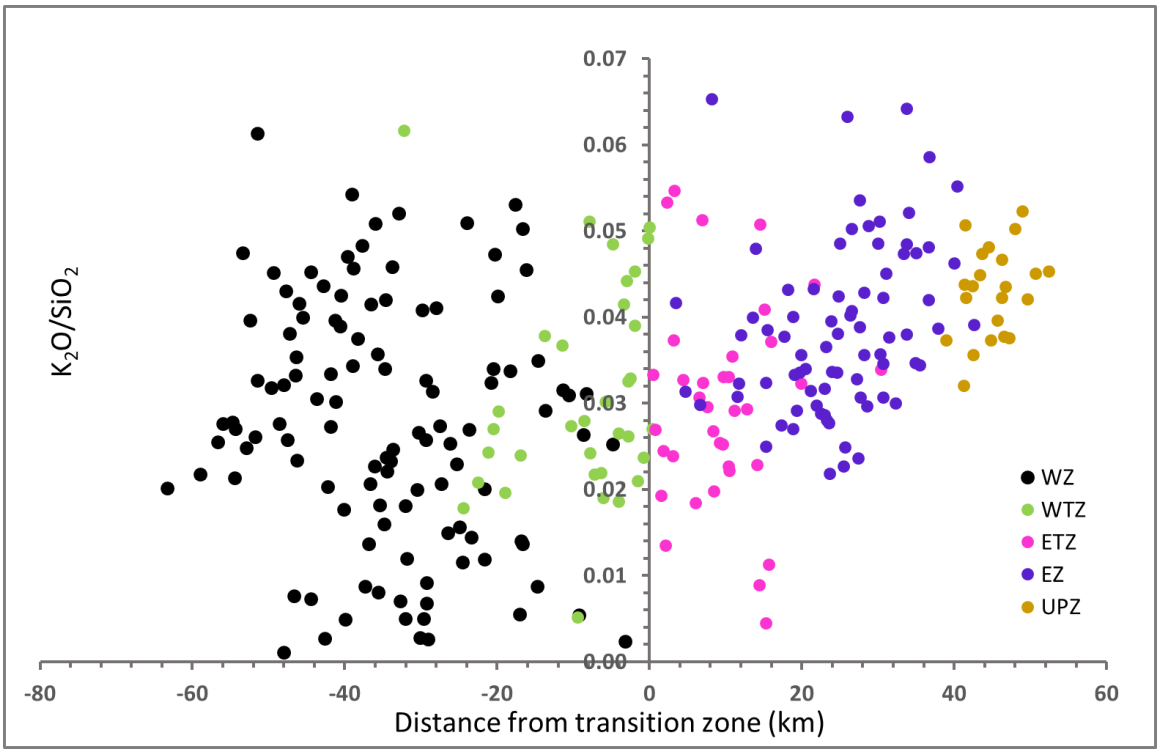

Figure 19. K_2O/SiO_2 vs. W-E distance from the transition zone dividing line with samples grouped by PRB zone. The west is characterized by wide variation while the east shows an increasing trend and is less variable.

Geochemical Interpolation Maps (2-D)

Interpolation maps capture more than simple west/east patterns, allowing visualization of second order geochemical spatial variation and revealing additional information about subduction zone processes not visible otherwise; in other words, they provide a 2-D or higher order variation view of patterns. In this section, ordinary kriging spatial interpolation is used to visualize detailed local variation, and trend surface analysis is used when visualization of large scale trends is not clear due to a high level of local heterogeneity (used for SiO_2 here). Interpolation output is a raster statistical surface that is displayed as contoured for Sr_i and smoothed for all the other maps.

It is important to note that interpolation introduces some averaging, resulting in a certain amount of contraction in the range of values. For example, the lowest SiO_2 interpolated value is 56 wt. % even though some gabbro samples have SiO_2 values as low as 43 wt. %.

Maps of Standard Geochemical Parameters

In this section, the four subduction zone geochemical processes are visualized spatially using their associated standard geochemical parameters, and the patterns are interpreted in terms of the subduction zone environment.

Visualization of SiO_2 spatial variation (**Figure 20 and 21**) reveals some interesting patterns. Generally, SiO_2 is bimodal in the west and moderately high in the east (best seen in **Figure 21**). Relatively high SiO_2 values in the western margin of the batholith corresponds to areas where sampling occurred at more felsic upper parts of plutons – near the pluton roof (Doug Morton, personal communication). A band of low values is found west of the transition line, corresponding to the region in which most gabbros are found. The eastern zone is characterized by relatively high SiO_2 composition in a part of the batholith interpreted to have been emplaced through continental crust in a compressional tectonic regime. This area is dominated by intermediate composition granodiorite and tonalite La Posta-style zoned plutons, such as the San Jacinto plutons. Recycling or reprocessing of existing continental material could be contributing to the increase in felsic composition of these rocks. In a model developed by Lee et al. (2007), a hydrated mantle wedge-derived basaltic melt rose and caused underplating and melting of the lower continental crust. The basaltic magma mixed with felsic continental material

and rose through thicker continental lithosphere in the east, producing the more felsic plutons. In the western PRB, the ascending magma rose through a thinner oceanic lithosphere with less mixing occurring.

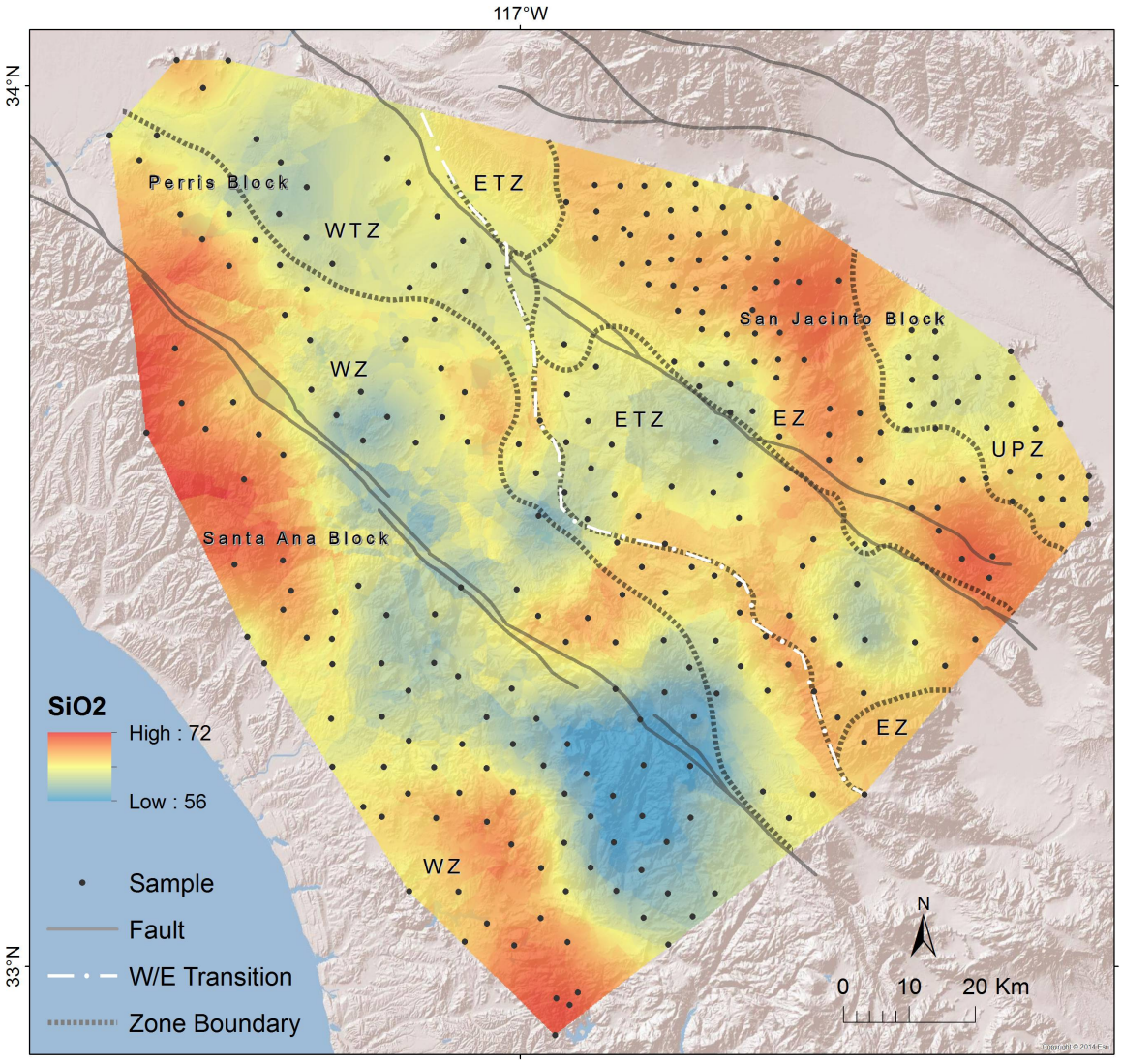

Figure 20. Spatial interpolation map of SiO_2 using kriging to indicate extent of differentiation; values in wt. %.

In comparison with the kriging interpolation, **Figure 21** uses trend surface analysis to focus visualization on the smoothed large scale trend for SiO_2 variation. A choice of 5^{th} order polynomial is a trade-off between being too general (lower order

polynomials) and showing too much detail (higher order polynomials). The general trend seen for the kriging interpolation of SiO_2 is nicely visualized without showing local heterogeneity.

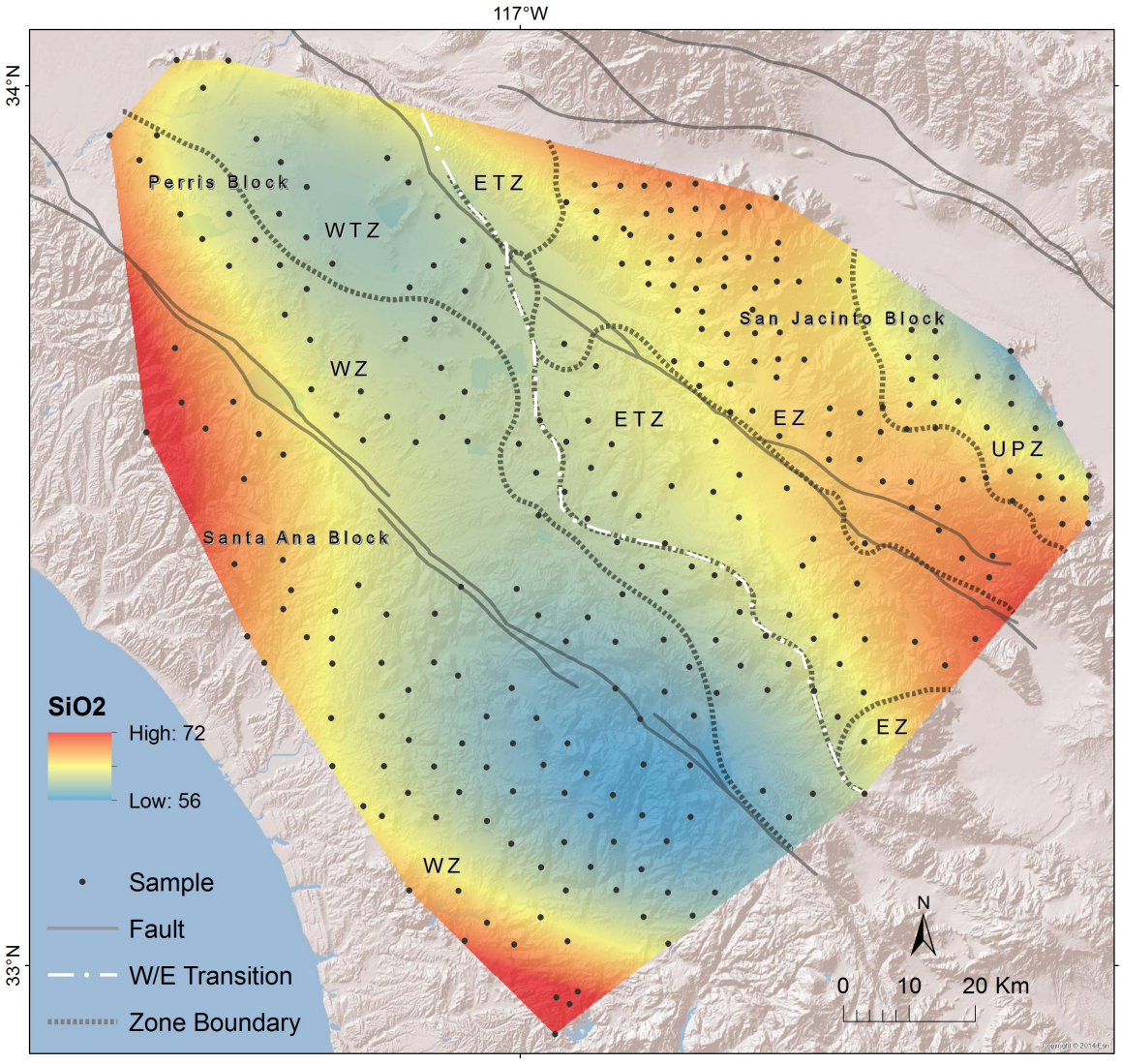

Figure 21. Spatial interpolation map of SiO_2 using trend surface analysis (5^{th} order polynomial) to indicate extent of differentiation; values in weight percent.

Initial strontium ranging from 0.703 in the west to 0.709 in the east is mapped in **Figure 22** and in Langenheim et al. (2004). Contouring is used here to show discrete

steps in the Sr_i trend. Increasing Sr_i from west to east suggests an increasing continental crust content, or crustal contamination. High Sr_i in the east (> 0.706) requires some degree of re-melting and assimilation of much older continental crust, meaning plutons in this region must have been emplaced through the ancient North American continental margin (Kistler, 1990; Kistler, 2003).

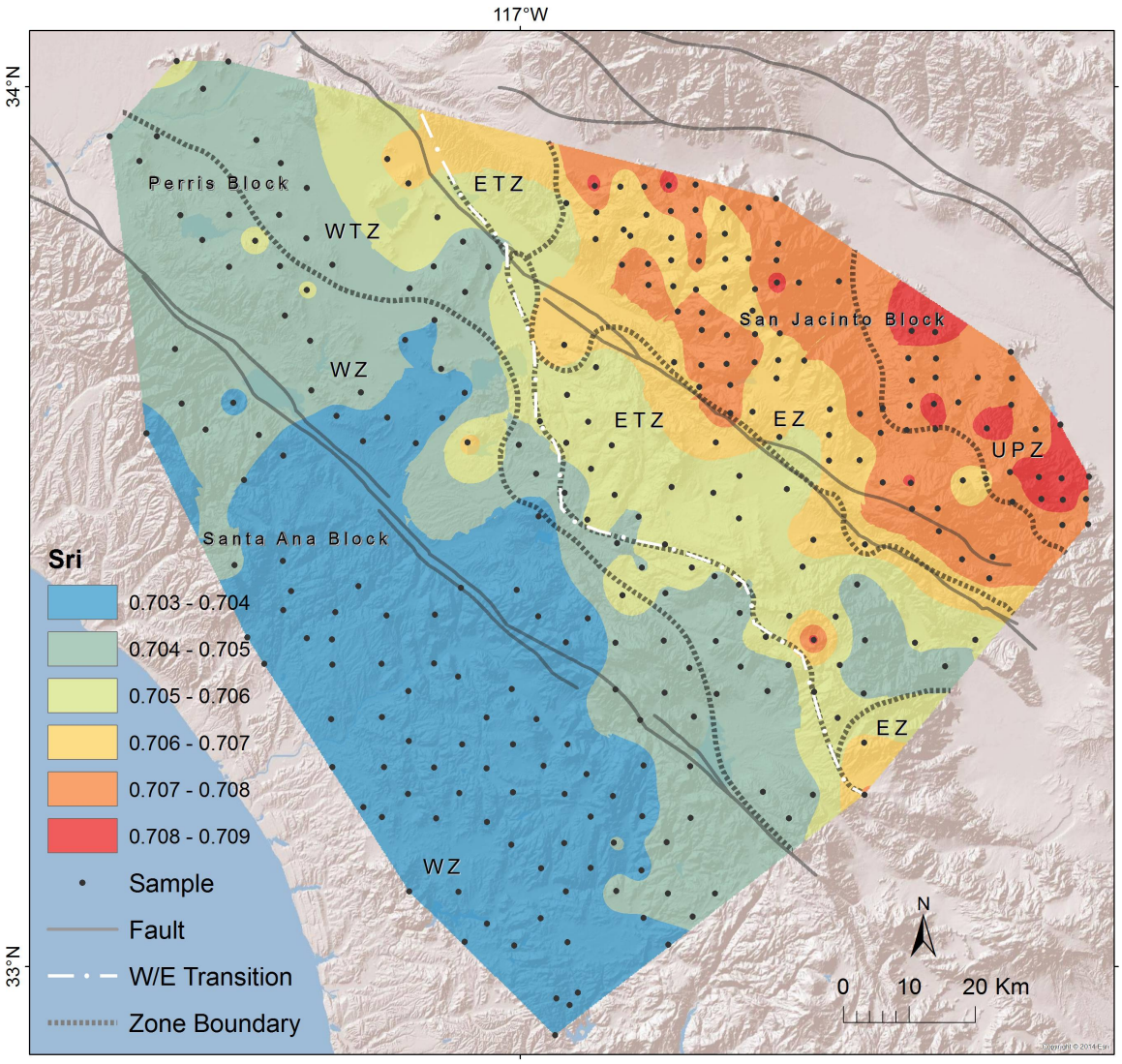

Figure 22. Spatial interpolation map of Sr_i to indicate crustal contamination.

Particularly low Sr_i (< 0.704) values in the Escondido plutons in the western zone indicate a lack of contamination from older continental crust since the basement is oceanic crust (Clausen et al., 2014).

The main Sr_i patterns to note are the low Sr_i values in the west, a gradual increase through the central transition zone and an abrupt increase at the San Jacinto fault zone. Several researchers have investigated the San Jacinto fault zone anomaly. Langenheim et al. (2004) looked at the prebatholithic environment of the PRB to try understand the development of the San Jacinto fault zone. A boundary running 1000 km along the batholith separates more mafic, higher density rocks on the west from relatively felsic lower density rocks in the east, strikes north-northwest towards the San Jacinto fault zone in the north and extends down to the mid-crust. The 0.706 initial strontium isopleth approximately follows the San Jacinto fault zone, with lower values in the west and higher values in the east. Sr_i values across the batholith are mostly independent of rock type, being geographically controlled and thus suggesting a prebatholithic origin. Langenheim et al. (2004) proposed an explanation for the steep initial strontium gradient across the San Jacinto fault zone as being due to the existence of separate blocks with differing geologic evolution before the emplacement of the batholith. Batholith emplacement then stitched across these preexisting features and magma contained their respective isotopic signatures.

Baird and Miesch (1984) noted that although chemical variation maps show continuous change from the southwest to the continental interior, the major discontinuity in modeled plutonic rock magma composition is located near the San Jacinto fault zone, in the Perris block.

Mapping Sr/Y variation reveals a spatial pattern of lower values in the west and higher values in the east, with the highest values occurring in the central part of the eastern transition zone and the northern part of the eastern zone, in the area of Mt. San Jacinto (**Figure 23**). A low region is found just south of the high values of Mt. San Jacinto, in the Palm Canyon area in the San Jacinto block, possibly relating to contamination by country rock.

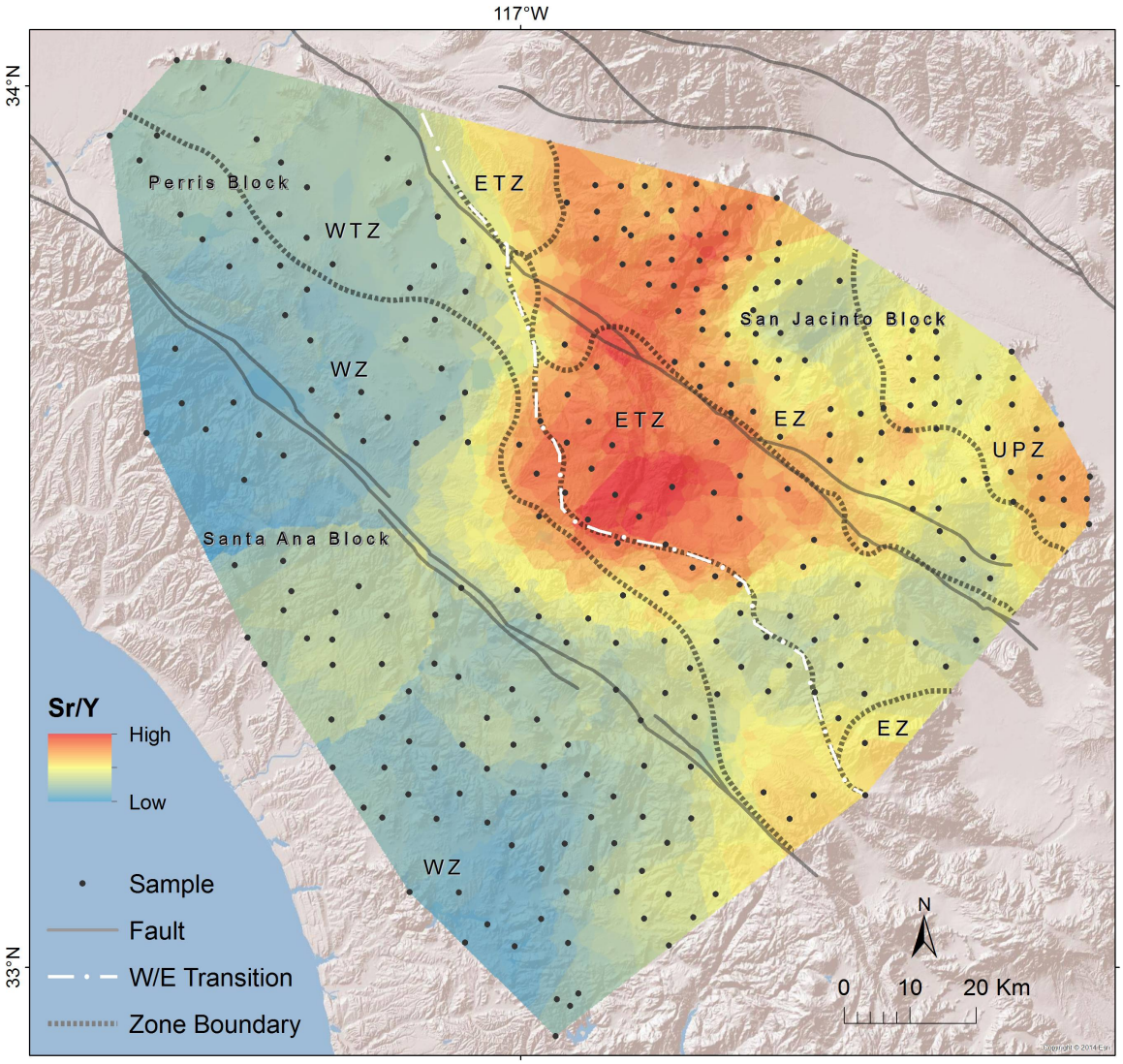

Figure 23. Spatial interpolation map of Sr/Y ratio to indicate magma source depth.

In the continental crust formation model of Lee et al. (2007), the mixture created by mantle wedge-derived melts mixing with lower continental crust, encountered thick continental lithosphere in the east, leaving behind a mafic garnet pyroxenite cumulate by fractional crystallization in the deep garnet stability zone. The effect of this garnet pyroxenite is reflected in the higher Sr/Y ratios in the plutons created by the complementary melts that ascended through the continental crust in parts of the east. The higher density mafic cumulates eventually delaminated and sank into the mantle, leaving behind a relatively felsic crust. In the west, shallower fractional crystallization did not develop the garnet pyroxenite cumulate, instead, olivine gabbros were fractionated.

The ratio of light to heavy REEs, represented by La/Yb, is another indicator of magma source depth (**Figure 24**). Higher values show a melt that is derived from the deeper garnet stability zone. Although this ratio only considers the fractionating effect of garnet on the REEs, a pattern similar to that of Sr/Y is seen.

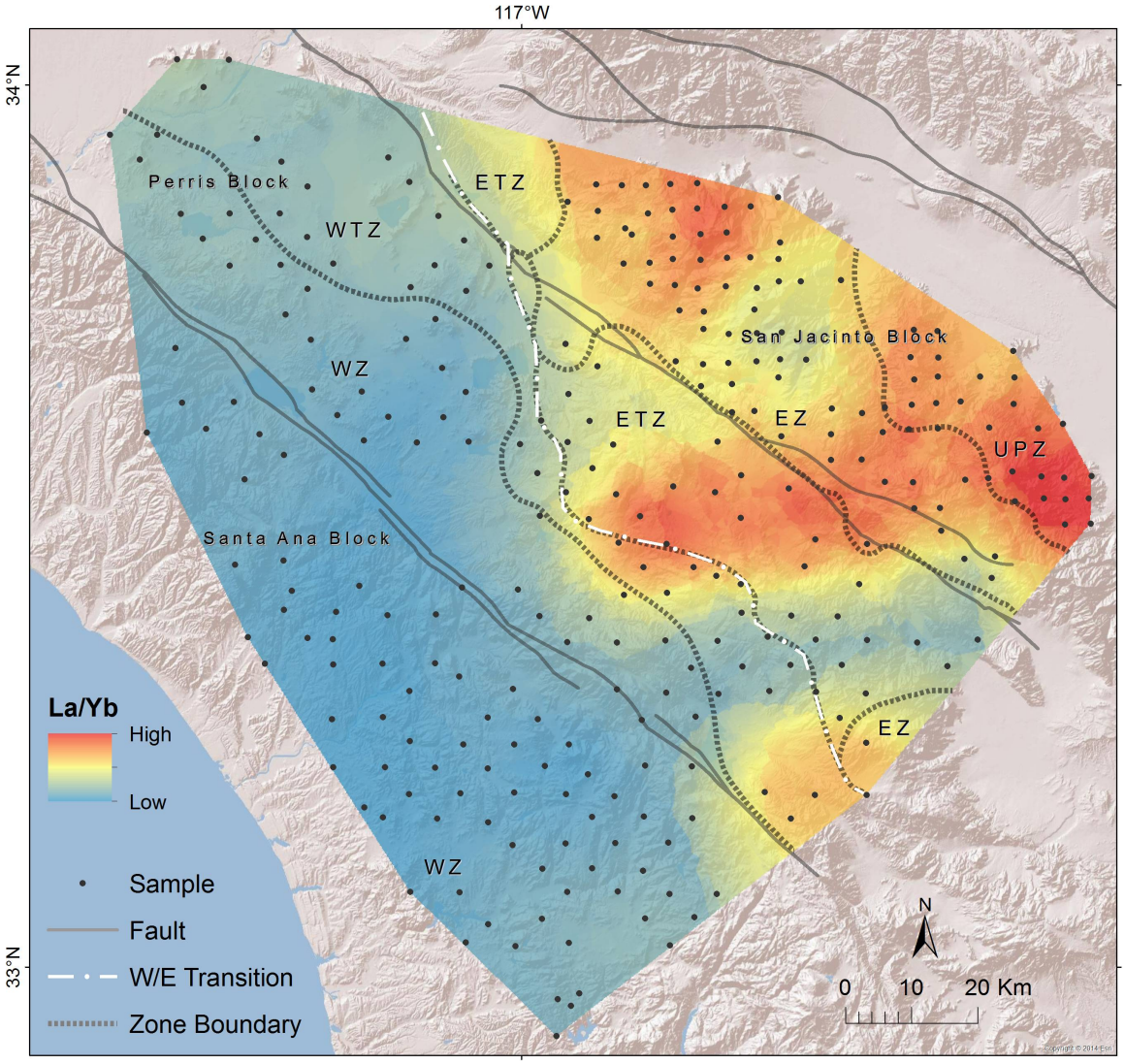

Figure 24. Spatial interpolation map of La/Yb ratio to indicate magma source depth.

The K_2O/SiO_2 ratio is associated with the level of magma alkalinity (Kuno, 1959). In **Figure 25**, the highest K_2O/SiO_2 concentrations are seen in the upper plate zone and eastern part of the eastern zone, possibly reflecting the K-h relationship of Kuno (1959). Another possible explanation for the far eastern areas of high alkalinity is greater mobility due to slab fluids transporting the water soluble potassium. Moderately high ratios observed in the north-west may be due to sampling the batholith at relatively high

positions – the pluton roof, similar to the pattern seen in the SiO_2 maps. The trough of low K_2O/SiO_2 ratios correspond roughly to the low SiO_2 values seen in **Figure 20** – locations with more mafic compositions and lower concentrations of incompatible potassium.

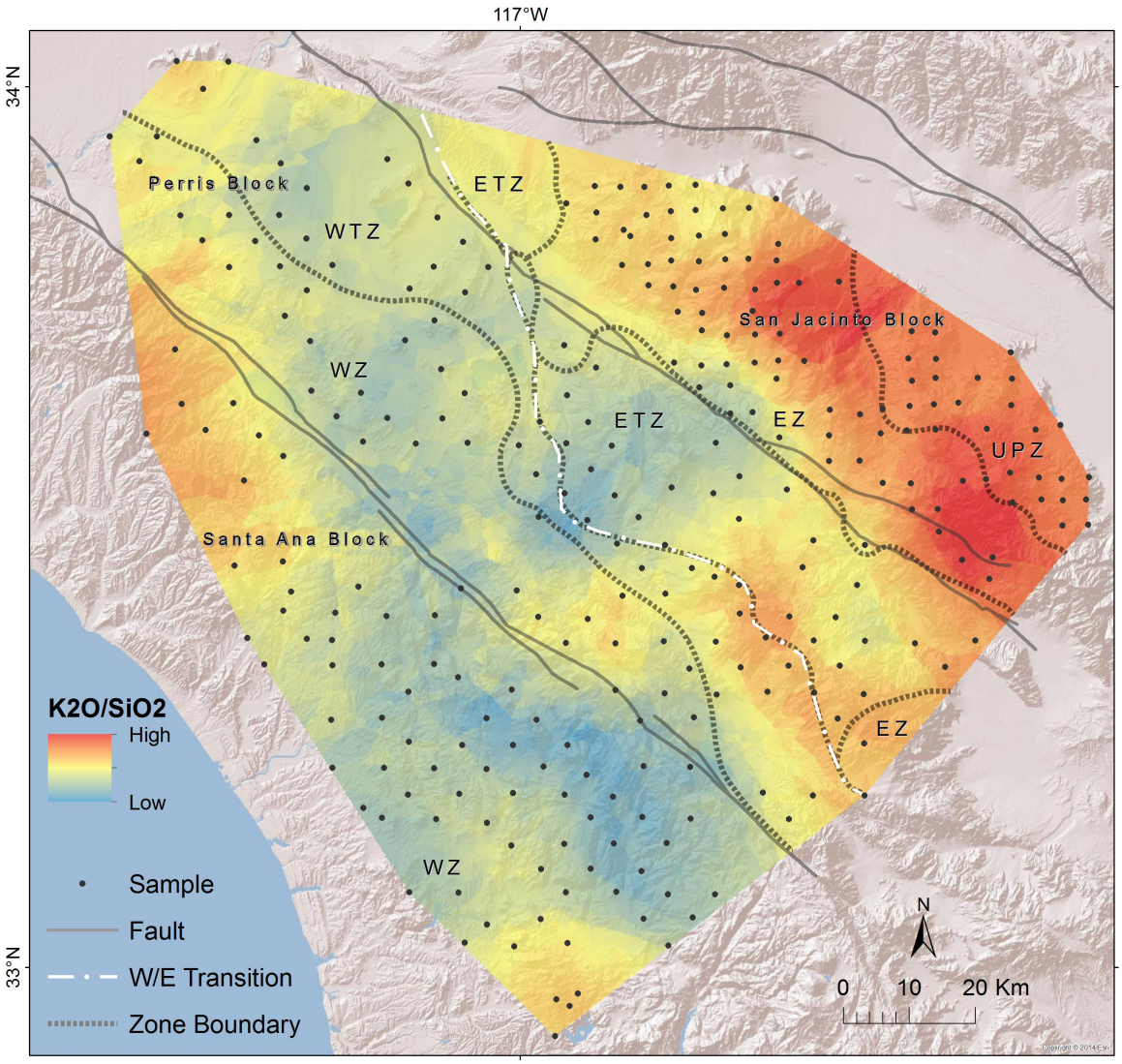

Figure 25. Spatial interpolation map of K_2O/SiO_2 to indicate alkalinity.

Maps of Principal Components

Principal components can be visualized spatially by mapping their scores. Spatial patterns in the three principal components described above are investigated here and compared visually to the standard geochemical parameter maps.

The first principal component as mapped in **Figure 26** accounts for 56.7% of explained variance and is interpreted as relating to extent of differentiation. Compared to the map of SiO_2 in **Figure 20**, some similarities can be seen. A trough of low values runs west of the transition line, coinciding with an area more mafic in composition with more gabbros. Values increase in the west where the batholith has been sampled at higher levels. The main difference is seen in the far east, where high values are seen east of the west/east transition line. This region has the highest concentration of incompatible elements, which is expected as it is interpreted to overlie the margin of the ancient North American craton. Ascending magma became increasingly felsic due to it having more more time for mixing with continental crust in the compressional tectonic environment and thicker lithosphere.

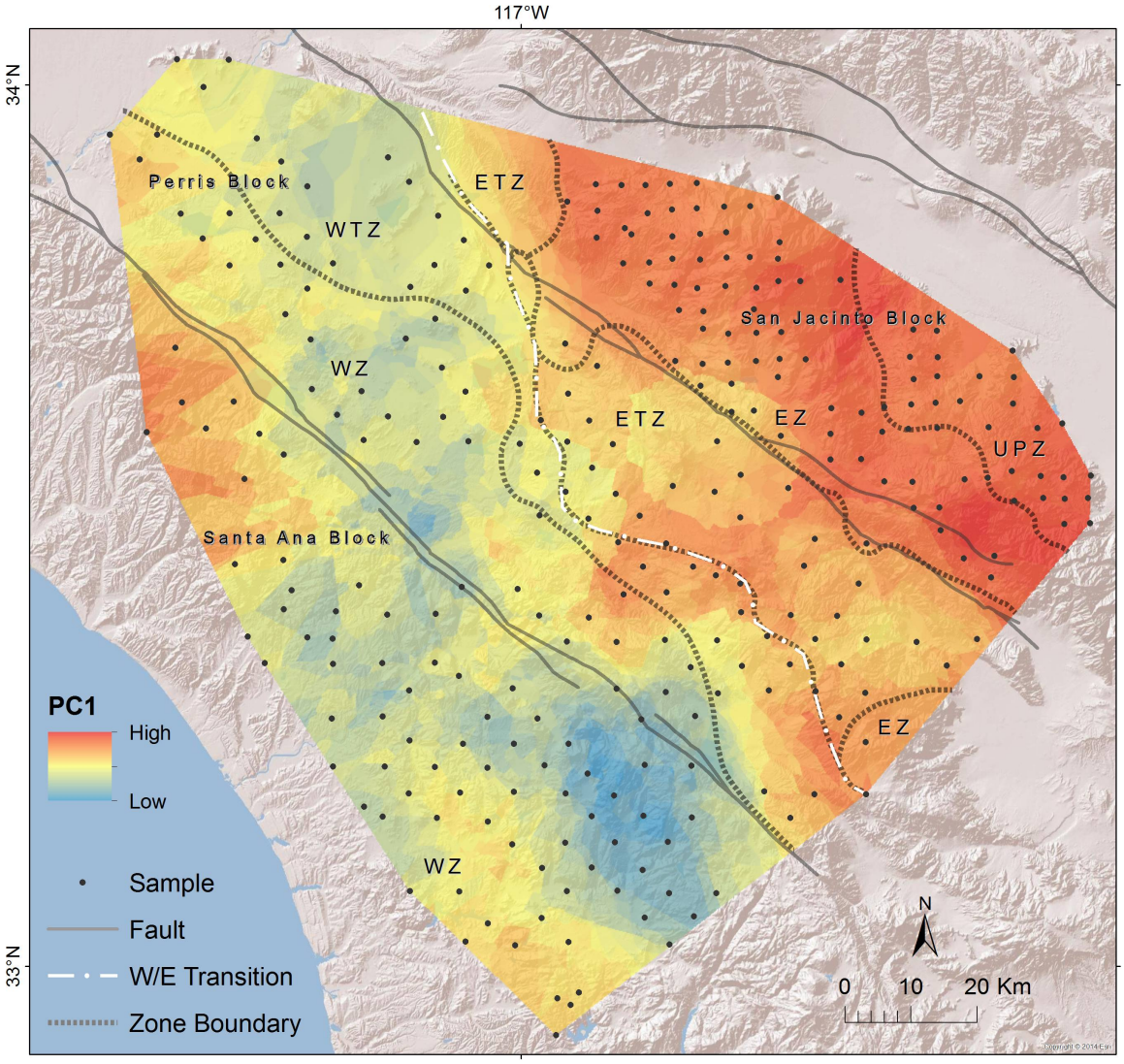

Figure 26. Spatial interpolation map of PC1 scores indicating the spatial variation of the interpreted extent of differentiation. The PC1 scores were inverted by multiplying with -1 for better comparison with **Figure 20**.

PC2, interpreted to be related to magma source depth, is mapped in **Figure 27**. Similar patterns to those found in the Sr/Y map in **Figure 23** can be seen, with high values indicating a deeper source in the central part of the eastern and western transition zones and along the northeastern margin of the batholith. In contrast to the Sr/Y map, higher values are seen in the northern and southern parts of the western and western

transition zones. The same low region seen in the Sr/Y map in the Palm Canyon area south of Mt. San Jacinto is found, possibly related to contamination by country rock.

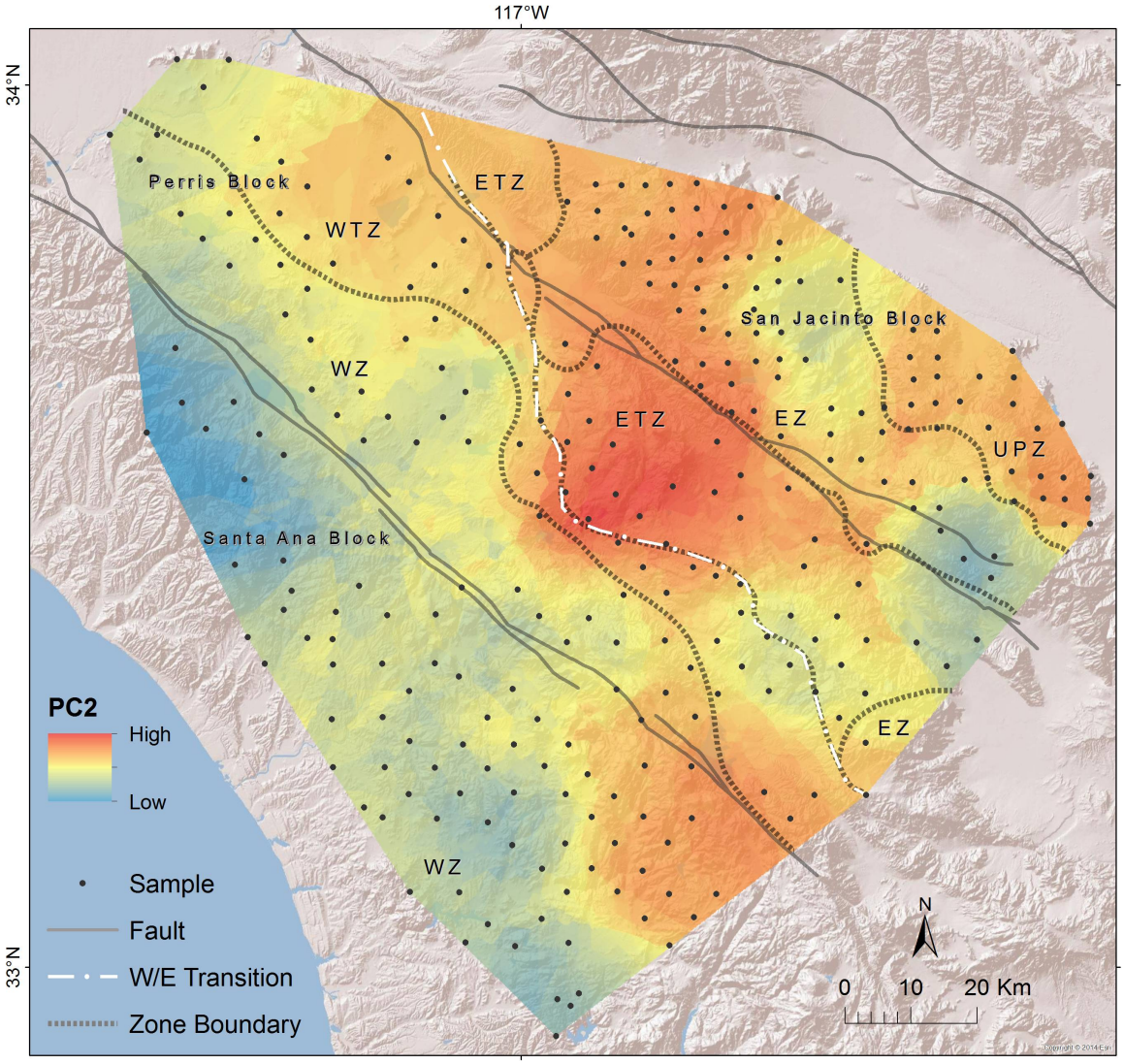

Figure 27. Spatial interpolation map of PC2 scores related to the spatial variation of the interpreted magma source depth.

Similar to the Sr/Y map a general trend of deepening magma source from west to east is visualized. This trend is also similar to that of the map of Sr_i in **Figure 22**. Local variation, especially in the Perris and San Jacinto blocks shows a much more complex

picture of magma source depth than a simple west-east trend. The weak west-east trends seen in **Figure 8** and **Figure 14** can be better understood when looking at the 2-D spatial variation.

The third principal component is mapped in **Figure 28**.

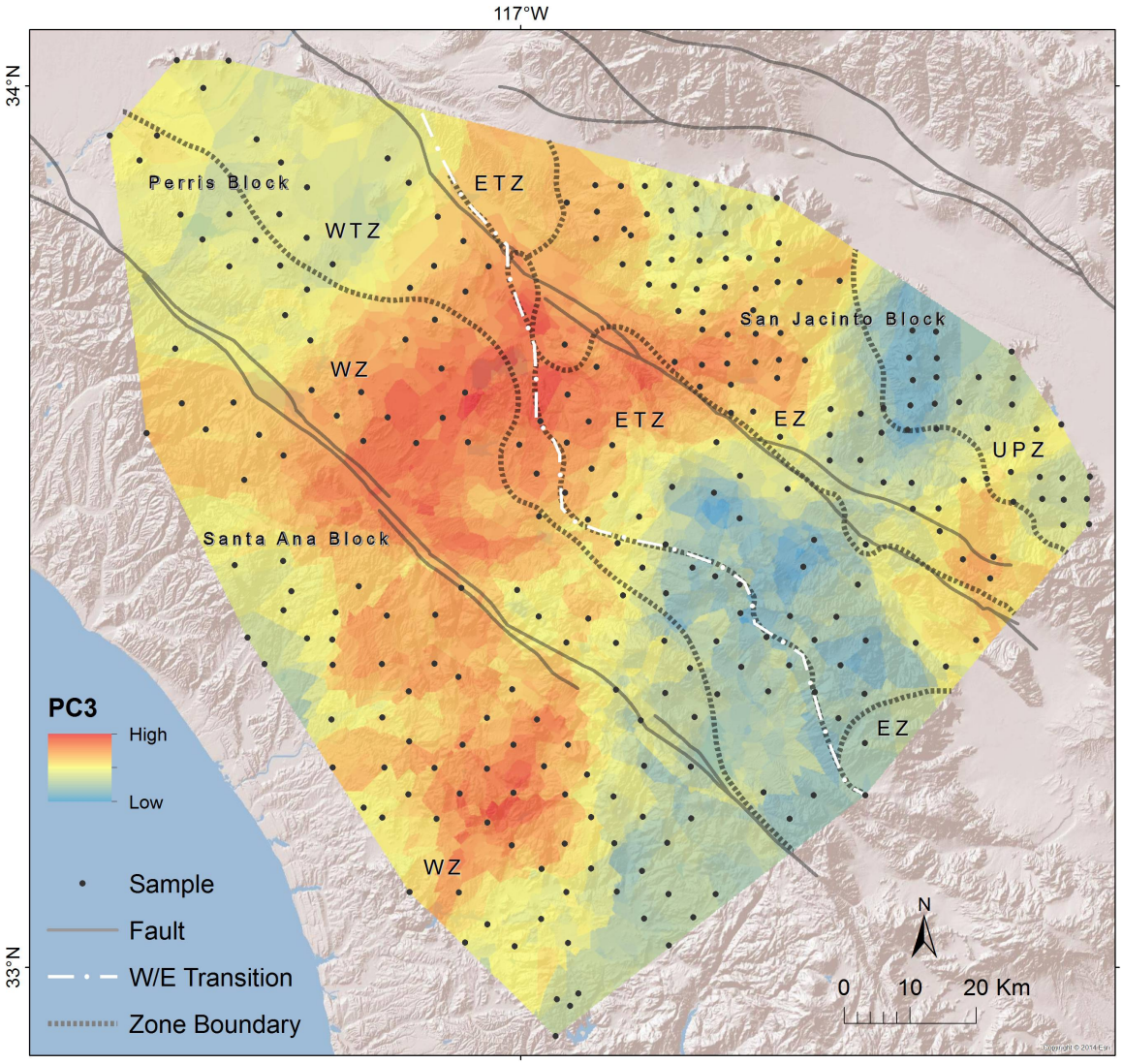

Figure 28. Spatial interpolation map of PC3 scores, with uncertain interpretation but possibly relating to element solubility/mobility.

A weak association with solubility was suggested from the biplot of PC2 vs. PC3 in **Figure 15**. Alkalinity is associated with highly water soluble and therefore mobile elements such as the alkali elements but is also a lot more complex. The pattern observed for PC3 does not resemble that observed for K_2O/SiO_2 and does not suggest a west/east trend. Therefore, PC3 representing only 6.7% of explained variance is possibly related to solubility and mobility, but it is not apparent that it is related to alkalinity. It possibly represents a combination of minor geological processes, including element solubility and mobility.

CHAPTER FOUR

CONCLUSIONS

Large igneous geochemical datasets have been assembled for subduction zone batholiths, especially along the American Cordilleran arc. One of the best such datasets, systematically sampled by Baird and Welday in the 1970s, has led to many new insights not only about the Peninsular Ranges batholith and Transverse Ranges, but about arc systems in general.

Since geochemical data are compositional in nature, they require special handling. In this case, the isometric log-ratio transformation was used to eliminate spurious relationships between variables. The opened geochemical data were analyzed using robust principal component analysis and the resulting three principal components were interpreted using biplots.

Looking at the arrangement of variables and samples with an understanding of magmatic geochemical principals led to the interpretation of the principal components as follows. The first principal component accounting for 56.7% of explained variance was interpreted to represent the extent of differentiation. The second principal component accounting for 17.3% of explained variance was interpreted to relate to magma source depth. The third principal component accounting for only 6.7% of explained variance possibly refers to solubility and mobility, but this is not clear. Altogether, the three principal components account for almost 81% of explained variance. A summary of the interpretations of PC1, PC2 and PC3 and the related standard parameters used to quantify the interpreted subduction zone process is given in **Table 3**.

Table 3. Interpretations of principal components and the relevant standard geochemical parameters.

Principal component	Interpretation	Standard Parameter
1	Extent of differentiation and crustal contamination	SiO_2 and Sr_i (Baird and Miesch, 1984; Faure and Powell, 2012; Kistler, 2003)
2	Magma source depth	Sr/Y and La/Yb (Profeta et al., 2015)
3	Solubility and mobility (weak)	K_2O/SiO_2 (Kuno, 1959; Winter, 2010)

If differentiation index is the extent to which felsic and mafic elements or minerals are separated from each other, then PC1 may be the best such index because it uses all of the elements rather than just some of them in the calculation.

Clusters of rare earth elements, along with Y and Sr in the PC1 vs. PC2 biplot show the fractionating effects of garnet and plagioclase at deep and intermediate shallow depths respectively. The heavy rare earth elements and Y are strongly fractionated into the solid at depth by garnet, while Sr is strongly fractionated into the solid at shallower levels by plagioclase. These fractionations result in the melt complement being depleted in those elements. Consequently, Sr/Y and the REEs can be used as geobarometers that reflect the average depth of magma generation. Likewise for PC2, however it has the benefit of considering relationships among all elements simultaneously, possibly being a more comprehensive index of magma source depth.

The standard geochemical parameters for several subduction zone processes were visualized spatially over the northern Peninsular Ranges batholith using 1-D west/east plots and 2-D interpolation maps. Multiple systematic west/east variation trends were noted and related to previous studies.

A bimodal pattern in the west was found for SiO_2 and extent of differentiation, while the east was generally higher and unimodal. Mapping the principal components showed similar patterns between PC1 and SiO_2. The dominant trend observed in the PC1 map is of the incompatible elements increasing from west to east and of the compatible elements decreasing in the same direction.

Magma source depth was visualized by mapping Sr/Y. Very similar spatial variation patterns were seen in the map of PC2, supporting the PC2 interpretation of magma source depth. A systematic deepening trend is noticed from a shallow, primitive source emplaced through oceanic crust in the west to a more evolved, deeper source emplaced through continental crust in the east. A similar trend is noticed by mapping Sr_i, that of increasing continental influence towards the east, with an abrupt increase near the San Jacinto fault zone.

The standard methods of analysis include bivariate plots and spider diagrams where subsets of geochemical elements are analyzed in isolation. The exploratory data analysis tools of multivariate analysis and spatial visualization open up new possibilities in understanding subduction zone geochemical datasets by giving a more holistic view of the data. Multivariate analysis allows all geochemical variables to be analyzed simultaneously, revealing relationships and interactions between all variables. Mapping of geochemistry parameters provides a way to explore the spatial variation of important subduction zone processes. Mapping of principal component scores assists in interpretation of PCA results and reveals spatial patterns that can help in identifying geochemical processes that are not otherwise visible.

REFERENCES

Abdi, H., and Williams, L. J., 2010, Principal component analysis: Wiley Interdisciplinary Reviews: Computational Statistics, v. 2, no. 4, p. 433-459.

Aitchison, J., 1986, The statistical analysis of compositional data.

Aitchison, J., and Greenacre, M., 2002, Biplots of compositional data: Journal of the Royal Statistical Society: Series C (Applied Statistics), v. 51, no. 4, p. 375-392.

Alférez, G. H., Rodríguez, J., Clausen, B., and Pompe, L., Interpreting the Geochemistry of Southern California Granitic Rocks using Machine Learning, *in* Proceedings Proceedings on the International Conference on Artificial Intelligence (ICAI)2015, The Steering Committee of The World Congress in Computer Science, Computer Engineering and Applied Computing (WorldComp), p. 592.

Baird, A. K., Baird, K. W., and Welday, E. E., 1979, Batholithic Rocks of the Northern Peninsular and Transverse Ranges, Southern California: Chemical Composition and Variation: Department of Geological Sciences San Diego State University.

Baird, A. K., and Miesch, A. T., 1984, Batholithic rocks of southern California-a model for the petrochemical nature of their source materials.: U. S. Geological Survey, p. 42.

Bateman, P., Clark, L., and Huber, N., 1963, Moore J. G., Reinhart C. D. (1963) The Sierra Nevada batholith–a synthesis of recent work across the central part: US Geol Surv Prof Pap D, v. 414.

Bostock, M., 2013, The Moho in subduction zones: Tectonophysics, v. 609, p. 547-557.

Bowen, N., 1922, The reaction principle in petrogenesis: The Journal of Geology, v. 30, no. 3, p. 177-198.

Buccianti, A., 2013, Is compositional data analysis a way to see beyond the illusion?: Computers & Geosciences, v. 50, p. 165-173.

Butler, A., Bierman, S., and Marion, G., 2005, Statistical methods for environmental risk assessment: Compositional data module. Biomathematics and Statistics Scotland, The University of Edinburgh, James Clerk Maxwell Building, The King's Buildings, Edinburgh EH9 3JZ.

Carranza, E. J. M., 2011, Analysis and mapping of geochemical anomalies using logratio-transformed stream sediment data with censored values: Journal of Geochemical Exploration, v. 110, no. 2, p. 167-185.

Carrol, M. R., and Wyllie, J., 1990, The system tonalite-H_20 at 15 kbar and the genesis of calc-alkaline magmas: American Mineralogist, v. 75, p. 345-357.

Chang, K.-T., 2013, Introduction to geographic information systems, Boston, McGraw-Hill Higher Education, xv, 432 p. p.:

Chapman, J. B., Ducea, M. N., DeCelles, P. G., and Profeta, L., 2015, Tracking changes in crustal thickness during orogenic evolution with Sr/Y: An example from the North American Cordillera: Geology, v. 43, no. 10, p. 919-922.

Chavez Jr, P. S., and Kwarteng, A. Y., 1989, Extracting spectral contrast in Landsat Thematic Mapper image data using selective principal component analysis: Photogrammetric Engineering and Remote Sensing, v. 55, no. 3, p. 339-348.

Chayes, F., 1971, Ratio correlation: a manual for students of petrology and geochemistry, University of Chicago Press.

Clausen, B., Martinez, A., Gonzalez, L., Poma, O., Paterson, S., and Ianno, A., Magma sources and mixing for the Coastal Batholith in southern Peru: insights from new elemental and isotopic data and from comparison with California batholithic rocks, *in* Proceedings AGU Fall Meeting Abstracts 2013, Volume 1, p. 2667.

Clausen, B., Martínez Ardila, A., and Morton, D., A Geochemical Comparison of the Northern Peninsular Ranges Batholith in Southern California and the Coastal Batholith in Southern Peru, *in* Proceedings AGU Fall Meeting Abstracts 2010, Volume 1, p. 2346.

Clausen, B. L., Morton, D. M., Kistler, R. W., and Lee, C.-T. A., 2014, Low-initial-Sr felsic plutons of the northwestern Peninsular Ranges batholith, southern California, and the role of mafic-felsic magma mixing in continental crust formation: Geological Society of America Memoirs, v. 211, p. 317-344.

Clemmer, G., 2013, The GIS 20 : essential skills, Redlands, California, Esri Press, xv, 185 pages p.:

Clinkenbeard, J., and Walawender, M., 1989, Mineralogy of the La Posta Pluton; implications for the origin of zoned plutons in the eastern Peninsular Ranges Batholith, Southern and Baja California: American Mineralogist, v. 74, no. 11-12, p. 1258-1269.

Condie, K. C., 2013, Plate tectonics & crustal evolution, Elsevier.

Davis, J. C., and Sampson, R. J., 1986, Statistics and data analysis in geology, Wiley New York et al.

De la Torre, F., and Black, M. J., Robust principal component analysis for computer vision, *in* Proceedings Computer Vision, 2001. ICCV 2001. Proceedings. Eighth IEEE International Conference on2001, Volume 1, IEEE, p. 362-369.

Ding, C., and He, X., K-means clustering via principal component analysis, *in* Proceedings Proceedings of the twenty-first international conference on Machine learning 2004, ACM, p. 29.

Eddy, W. F., 1977, A new convex hull algorithm for planar sets: ACM Transactions on Mathematical Software (TOMS), v. 3, no. 4, p. 398-403.

Egozcue, J. J., Pawlowsky-Glahn, V., Mateu-Figueras, G., and Barcelo-Vidal, C., 2003, Isometric logratio transformations for compositional data analysis: Mathematical Geology, v. 35, no. 3, p. 279-300.

Engle, M. A., and Blondes, M. S., 2014, Linking compositional data analysis with thermodynamic geochemical modeling: Oilfield brines from the Permian Basin, USA: Journal of Geochemical Exploration, v. 141, p. 61-70.

Esri, 2016, ArcGIS for Desktop: https://www.arcgis.com: Redlands, CA.

Faure, G., and Powell, J. L., 2012, Strontium isotope geology, Springer Science & Business Media.

Filzmoser, P., and Hron, K., 2008, Outlier detection for compositional data using robust methods: Mathematical Geosciences, v. 40, no. 3, p. 233-248.

Filzmoser, P., Hron, K., and Reimann, C., 2009, Principal component analysis for compositional data with outliers: Environmetrics, v. 20, no. 6, p. 621-632.

Flood, R., Orford, J., McKinley, J., and Roberson, S., 2015, Effective grain size distribution analysis for interpretation of tidal–deltaic facies: West Bengal Sundarbans: Sedimentary Geology, v. 318, p. 58-74.

Gabriel, K. R., 1971, The biplot graphic display of matrices with application to principal component analysis: Biometrika, v. 58, no. 3, p. 453-467.

Goldschmidt, V. M., 1937, The principles of distribution of chemical elements in minerals and rocks. The seventh Hugo Müller Lecture, delivered before the Chemical Society on March 17th, 1937: Journal of the Chemical Society (Resumed), p. 655-673.

Greenwood, N. N., and Earnshaw, A., 2012, Chemistry of the Elements, Elsevier.

Gromet, L. P., and Silver, L. T., 1987, Ree Variations across the Peninsular Ranges Batholith - Implications for Batholithic Petrogenesis and Crustal Growth in Magmatic Arcs: Journal of Petrology, v. 28, no. 1, p. 75-125.

Grove, T. L., Till, C. B., and Krawczynski, M. J., 2012, The role of H_2O in subduction zone magmatism: Annual Review of Earth and Planetary Sciences, v. 40, p. 413-439.

Grunsky, E. C., 2010, The interpretation of geochemical survey data: Geochemistry-Exploration Environment Analysis, v. 10, no. 1, p. 27-74.

Grunsky, E. C., Mueller, U. A., and Corrigan, D., 2014, A study of the lake sediment geochemistry of the Melville Peninsula using multivariate methods: Applications for predictive geological mapping: Journal of Geochemical Exploration, v. 141, p. 15-41.

Hawkesworth, C., Rogers, N., Van Calsteren, P., and Menzies, M., 1984, Mantle enrichment processes: Nature, v. 311, no. 5984, p. 331-335.

Helsel, D. R., 1990, Less than obvious-statistical treatment of data below the detection limit: Environmental Science & Technology, v. 24, no. 12, p. 1766-1774.

Hill, R. I., 1984, Petrology and Petrogenesis of Batholithic Rocks, San Jacinto Mountains, Southern California [Ph.D.: California Institute of Technology], 660 p.

Hobbs, D., and Edwards, T., 1994, Solubility of uranium in alkaline salt solutions: Westinghouse Savannah River Co., Aiken, SC (United States).

Hofmann, A. W., 1988, Chemical differentiation of the Earth: the relationship between mantle, continental crust, and oceanic crust: Earth and Planetary Science Letters, v. 90, no. 3, p. 297-314.

Hubert, M., and Engelen, S., 2004, Robust PCA and classification in biosciences: Bioinformatics, v. 20, no. 11, p. 1728-1736.

James, B. R., 1996, Peer reviewed: the challenge of remediating chromium-contaminated soil: Environmental Science & Technology, v. 30, no. 6, p. 248A-251A.

Jolliffe, I., 2014, Principal Component Analysis, Wiley StatsRef: Statistics Reference Online, John Wiley & Sons, Ltd.

Joreskog, K. G., Klovan, J. E., and Reyment, R. A., 1976, Geological factor analysis, Elsevier Scientific Pub. Co.

Kistler, R. W., 1990, Two different lithosphere types in the Sierra Nevada, California: Geological Society of America Memoirs, v. 174, p. 271-282.

Kistler, R. W., et al., 2003, Isotopes and ages in the northern Peninsular Ranges batholith, southern California.: U. S. Geological Survey Open-File Report, v. 03, p. 45.

Kistler, R. W., Wooden, J. L., Premo, W. R., and Morton, D. M., 2014, Pb-Sr-Nd-O isotopic characterization of Mesozoic rocks throughout the northern end of the Peninsular Ranges batholith: Isotopic evidence for the magmatic evolution of oceanic arc–continental margin accretion during the Late Cretaceous of southern California: Geological Society of America Memoirs, v. 211, p. 263-316.

Klovan, J., 1975, R-and Q-mode factor analysis, Concepts in geostatistics, Springer, p. 21-69.

Kucera, M., and Malmgren, B. A., 1998, Logratio transformation of compositional data: a resolution of the constant sum constraint: Marine Micropaleontology, v. 34, no. 1, p. 117-120.

Kuno, H., 1959, Origin of Cenozoic petrographic provinces of Japan and surrounding areas: Bulletin Volcanologique, v. 20, no. 1, p. 37-76.

Langenheim, V. E., Jachens, R. C., and Aiken, C., 2014, Geophysical framework of the Peninsular Ranges batholith—Implications for tectonic evolution and neotectonics: Geological Society of America Memoirs, v. 211, p. 1-20.

Langenheim, V. E., Jachens, R. C., Morton, D. M., Kistler, R. W., and Matti, J. C., 2004, Geophysical and isotopic mapping of preexisting crustal structures that influenced the location and development of the San Jacinto fault zone, southern California: Geological Society of America Bulletin, v. 116, no. 9-10, p. 1143-1157.

Larsen, E. S., 1948, Batholith and associated rocks of Corona, Elsinore, and San Luis Rey quadrangles southern California: Geological Society of America Memoirs, v. 29, p. 1-185.

Le Maitre, R. W., Streckeisen, A., Zanettin, B., Le Bas, M., Bonin, B., and Bateman, P., 2005, Igneous rocks: a classification and glossary of terms: recommendations of the International Union of Geological Sciences Subcommission on the Systematics of Igneous Rocks, Cambridge University Press.

Lee, C.-T. A., Morton, D. M., Kistler, R. W., and Baird, A. K., 2007, Petrology and tectonics of Phanerozoic continent formation: from island arcs to accretion and continental arc magmatism: Earth and Planetary Science Letters, v. 263, no. 3, p. 370-387.

Leeman, W. P., 1983, The influence of crustal structure on compositions of subduction-related magmas: Journal of Volcanology and Geothermal Research, v. 18, no. 1, p. 561-588.

Martinez, A., Clausen, B., Gonzalez, L., and Poma, O., Field relationships and petrographic evidence of magma mingling and mixing processes in the Arequipa Segment of the Coastal Batholith in Southern Peru, *in* Proceedings AGU Fall Meeting Abstracts 2013, Volume 1, p. 2671.

Mertler, C. A., and Vannatta, R. A., 2002, Advanced and multivariate statistical methods: Los Angeles, CA: Pyrczak.

Miesch, A., 1976, Interactive computer programs for petrologic modeling with extended Q-mode factor analysis: Computers & Geosciences, v. 2, no. 4, p. 439-492.

Miller, F. K., Morton, D. M., and Premo, W. R., 2014, Potassium-argon cooling ages in the northern part of the Peninsular Ranges batholith and offsets on the Elsinore and San Jacinto fault zones: Geological Society of America Memoirs, v. 211, p. 181-198.

Miller, M., 2014, Cretaceous batholiths and roof pendants, http://geologictimepics.com.

Morton, D. M., Baird, A. K., and Baird, K. W., 1969, Lakeview Mountains Pluton, Southern California Batholith .2. Chemical Composition and Variation: Geological Society of America Bulletin, v. 80, no. 8, p. 11.

Morton, D. M., Miller, F. K., Kistler, R. W., Premo, W. R., Lee, C.-T. A., Langenheim, V. E., Wooden, J. L., Snee, L. W., Clausen, B. L., and Cossette, P., 2014, Framework and petrogenesis of the northern Peninsular Ranges batholith, southern California: Geological Society of America Memoirs, v. 211, p. 61-143.

Morton, D. M., Wadsworth, W., and Zenger, D., 1985, Memorial to Alexander Kennedy Baird 1932-1985: ftp://rock.geosociety.org/pub/Memorials/v18/Baird-AK.pdf.

Neocleous, T., Aitken, C., and Zadora, G., 2011, Transformations for compositional data with zeros with an application to forensic evidence evaluation: Chemometrics and Intelligent Laboratory Systems, v. 109, no. 1, p. 77-85.

Ortega-Rivera, A., 2003, Geochronological constraints on the tectonic history of the Peninsular Ranges Batholith of Alta and Baja California: Tectonic implications for western México: Geological Society of America Special Papers, v. 374, p. 297-335.

Otamendi, J. E., Jesús, D., Douce, A. E. P., and Castro, A., 2002, Rayleigh fractionation of heavy rare earths and yttrium during metamorphic garnet growth: Geology, v. 30, no. 2, p. 159-162.

Paterson, S. R., and Ducea, M. N., 2015, Arc magmatic tempos: gathering the evidence: Elements, v. 11, no. 2, p. 91-98.

Paterson, S. R., Okaya, D., Memeti, V., Economos, R., and Miller, R. B., 2011, Magma addition and flux calculations of incrementally constructed magma chambers in continental margin arcs: Combined field, geochronologic, and thermal modeling studies: Geosphere, v. 7, no. 6, p. 1439-1468.

Pawlowsky-Glahn, V., and Buccianti, A., 2011, Compositional data analysis theory and applications: Hoboken, N.J., Wiley.

Pawlowsky-Glahn, V., Egozcue, J. J., and Tolosana Delgado, R., 2007, Lecture notes on compositional data analysis: Tech. rep., Universitat de Girona, Spain.

Pearson, K., 1897, Mathematical contributions to the theory of evolution. On the law of ancestral heredity: Proceedings of the Royal Society of London, v. 62, no. 379-387, p. 386-412.

Profeta, L., Ducea, M. N., Chapman, J. B., Paterson, S. R., Gonzales, S. M. H., Kirsch, M., Petrescu, L., and DeCelles, P. G., 2015, Quantifying crustal thickness over time in magmatic arcs: Scientific reports, v. 5.

R-development-core-team, 2016, R: A language and environment for statistical computing: Vienna, http://www.r-project.org.

Railsback, B., 2012, Earth Scientist's Periodic Table of the Elements and Their Ions, *in* http://www.gly.uga.edu/railsback/PT/815PeriodicTable48e029834.jpg, ed.: Athens, Georgia, University of Georgia.

Reimann, C., Filzmoser, P., Fabian, K., Hron, K., Birke, M., Demetriades, A., Dinelli, E., Ladenberger, A., and Team, T. G. P., 2012, The concept of compositional data analysis in practice—total major element concentrations in agricultural and grazing land soils of Europe: Science of the Total Environment, v. 426, p. 196-210.

Ringwood, A., 1955, The principles governing trace element distribution during magmatic crystallization Part I: The influence of electronegativity: Geochimica et Cosmochimica Acta, v. 7, no. 3, p. 189-202.

Rollinson, H. R., 1993, Using geochemical data: evaluation, presentation, interpretation, Routledge.

Sharp, R. V., 1967, San Jacinto Fault Zone in the Peninsular Ranges of Southern California: Geological Society of America Bulletin, v. 78, no. 6, p. 705-730.

Sharp, Z. D., 1990, A laser-based microanalytical method for the in situ determination of oxygen isotope ratios of silicates and oxides: Geochimica et Cosmochimica Acta, v. 54, no. 5, p. 1353-1357.

Silver, L., and Chappell, B., 1988, The Peninsular Ranges Batholith: an insight into the evolution of the Cordilleran batholiths of southwestern North America: Transactions of the Royal Society of Edinburgh: Earth Sciences, v. 79, no. 2-3, p. 105-121.

Silver, L., Taylor, H., and Chappell, B., 1979, Some petrological, geochemical, and geochronological observations of the Peninsular Ranges batholith near the international border of the USA and Mexico, *in* Proceedings Mesozoic Crystalline Rocks: Geological Society of America, Annual Meeting, Guidebook, p. 83-110.

Sun, S.-S., and McDonough, W., 1989, Chemical and isotopic systematics of oceanic basalts: implications for mantle composition and processes: Geological Society, London, Special Publications, v. 42, no. 1, p. 313-345.

Symons, D. T. A., Walawender, M. J., Smith, T. E., Molnar, S. E., Harris, M. J., and Blackburn, W. H., 2003, Paleomagnetism and geobarometry of the La Posta Pluton, California: Geological Society of America Special Papers, v. 374, p. 135-155.

Tatsumi, Y., and Eggins, S., 1995, Subduction zone magmatism, Wiley.

Templ, M., Filzmoser, P., and Hron, K., 2009, Robust Imputation of Missing Values in Compositional Data using the R-Package robCompositions: New Techniques and Technologies for Statistics, Brussels.

Templ, M., Hron, K., and Filzmoser, P., 2016, RobCompositions: https://github.com/matthias-da/robCompositions.

Thirlwall, M., and Jones, N., 1983, Isotope geochemistry and contamination mechanics of Tertiary lavas from Skye, Northwest Scotland: Continental basalts and mantle xenoliths, p. 186-208.

Tilley, C., 1950, Some aspects of magmatic evolution: Quarterly Journal of the Geological Society, v. 106, no. 1-4, p. 37-61.

Tulloch, A. J., and Kimbrough, D. L., 2003, Paired plutonic belts in convergent margins and the development of high Sr/Y magmatism: Peninsular Ranges Batholith of Baja California and Median Batholith of New Zealand: Geological Society of America Special Papers, v. 374, p. 275-295.

USGS, 2016, California geologic map data, Volume 2016, USGS.

Van den Boogaart, K. G., and Tolosana-Delgado, R., 2013, Analyzing compositional data with R, Springer.

Vu, V. Q., 2016, Ggbiplot: https://github.com/vqv/ggbiplot.

Walawender, M., Gastil, R., Clinkenbeard, J., McCormick, W., Eastman, B., Wernicke, R., Wardlaw, M., Gunn, S., and Smith, B., 1990, Origin and evolution of the zoned La Posta-type plutons, eastern Peninsular Ranges batholith, southern and Baja California: Geological Society of America Memoirs, v. 174, p. 1-18.

White, W. M., 2013, Geochemistry, John Wiley & Sons.

Winter, J. D., 2010, Principles of igneous and metamorphic petrology, Prentice Hall New York.

APPENDIX ONE

RELATED FIELD WORK

Since this analysis uses a comprehensive systematically sampled geochemical dataset, not much value would be added by collecting more samples in the northern Peninsular Ranges batholith. I was able to gain relevant fieldwork experience by joining a month long field trip to sample the Cretaceous Peruvian Coastal batholith in the Peruvian Andean section of the Cordilleran arc. This arc segment has several characteristics in common with the northern Peninsular Ranges batholith as well as differences (Clausen et al., 2013; Clausen et al., 2010; Martinez et al., 2013). Similar to the Peninsular Ranges batholith, subduction progressed from west to east with an increasing depth trend to the east. The younging trend is also towards the east, approximately similar to the Peninsular Ranges batholith.

Two main goals for sampling were firstly to establish a baseline for stable oxygen isotopes by sampling unaltered rock over three transects, and secondly to estimate the amount and origin of hydrothermal fluid involved in potentially cooling the batholith. Sampling was done over three transects of the Peruvian Coastal batholith, in the north near Huacho (approximately 200 km north of Lima), in the Ica central area (approximately 300 km south of Lima) and in the south around Arequipa (approximately 1000 km south of Lima). The sampling strategy involved firstly planning from which units to collect samples using geological maps and papers detailing work previously done in the area. Outcrops were identified that offered relatively fresh exposures of the units required, accessed by roads or trails in the mountains or river valleys. Major river valleys with roads cutting into the Peruvian Coastal batholith and up into the Andes offered the

most convenient access. A sample of about 1 kg in weight was chipped off using a rock hammer and trimmed to fit in a sample bag. Both the bag and rock sample were labeled. Similar to the sampling done in the PRB, rock types collected included gabbro, tonalite, granodiorite and granite. Some monzogabbro and volcanic units were also sampled.

The altered samples were collected in the region of the central transect near Ica. A total of 106 mostly granitic and several volcanic samples were collected. The same sampling method was used; however areas of alteration were specifically targeted.

APPENDIX TWO

RELATED LAB WORK

The PRB geochemical data were originally analyzed by Baird and Miesch (1984). The samples were subsequently re-analyzed in the USGS lab in Denver, Colorado using X-ray fluorescence (XRF) analysis for major elements and inductively coupled plasma mass spectrometry (ICP-MS) analysis for trace elements (Morton et al., 2014). Isotopes were analyzed by R.W. Kistler and J. L. Wooden (Kistler, 2003).

The Peru samples were analyzed for elemental geochemistry at SGS labs in Canada. I assisted with laboratory analysis of stable oxygen and hydrogen isotopes. This involved first separating minerals from the sample and then analyzing each mineral containing oxygen or hydrogen at the stable isotope laboratory at California State University, Long Beach. Samples that contained larger mineral grains were separated by hand, while samples that contained very small crystals were sent to a lab in China for mineral separation. The lab analysis for oxygen stable isotopes involved equipment based on the laser fluorination method (Sharp, 1990). A small amount of sample (2-3 mg) is placed in a nickel sample holder and completely vaporized in a reaction chamber with a laser in the presence of bromine pentafluoride. After a few more processing steps, the oxygen isotopes ratios are measured using a mass spectrometer.

Zircons were analyzed for uranium-lead geochronology at the Arizona LaserChron Center at the University of Arizona, Tucson. A Laser Ablation Inductively Coupled Plasma Mass Spectrometry (LA-ICPMS) instrument was used to date samples from the Peruvian Coastal batholith over the course of several days. Before geochronological analysis could be undertaken, samples were sent to China for zircon

separation and then imaging of the zircons was done using cathodoluminescence at California State University, Northridge.